

THESIS

ANALYSIS OF VARIATIONS IN CHANNEL WIDTH AND SEDIMENT SUPPLY ON RIFFLE-  
POOL DYNAMICS, BEFORE AND AFTER DAM REMOVAL

Submitted by

Andrew K. Brew

Department of Civil and Environmental Engineering

In partial fulfillment of the requirements

For the Degree of Master of Science

Colorado State University

Fort Collins, Colorado

Summer 2014

Master's Committee:

Advisor: Peter A. Nelson

Brian P. Bledsoe  
Ellen E. Wohl

Copyright by Andrew K. Brew 2014

All Rights Reserved

## ABSTRACT

### ANALYSIS OF VARIATIONS IN CHANNEL WIDTH AND SEDIMENT SUPPLY ON RIFFLE- POOL DYNAMICS, BEFORE AND AFTER DAM REMOVAL

Many gravel-bed rivers feature quasi-regular alternations of shallow and deep areas known as riffle-pool sequences, which in straight reaches are often forced by variations in channel width. The mechanisms responsible for the formation and maintenance of riffle-pool sequences are still poorly understood. There is also much uncertainty in the basic understanding of how fluvial systems respond and readjust to large sediment fluxes through time (i.e. dam removal). Here we present physical experiments, numerical modeling, and field observations aimed at improving our understanding of how downstream variations in channel width affect bed morphology and influence riffle-pool development, and how these features respond to changes in sediment supply.

A two-dimensional morphodynamic model, Nays2D, has been used to explore interactions between the flow field, the sediment transport field, and the bed morphology for a channel with sinusoidal variations in width. Model predictions suggest that riffles form in wide sections of the channel while pools develop in channel constrictions, and these model results have been used to guide mobile-bed experiments we have conducted in a 21-cm wide, 9-m long flume. Artificial walls imposing a sinusoidal width variation have been installed in the flume, and during the experiments it is supplied with a constant water discharge and a sediment mixture of coarse sand and fine gravel. After riffles and pools developed under these equilibrium conditions, the sediment supply is increased during two experimental designs that simulate characteristics of a dam removal. The first

experiment examined increasing sediment supply to an original equilibrium rate after a period of starvation. The second introduces a well sorted sediment pulse that was four times greater than the equilibrium feed rate. This pulse of sediment evolved primarily through dispersion, rather than translation. These physical and numerical experiments are complemented by observations from a natural experiment on the Elwha River in Washington State, where the largest dam-removal project in history is providing riffle-pool sequences with greatly increased sediment supply. Analysis of aerial imagery and repeat bathymetric measurements indicate that prior to dam removal, pools on the Elwha were co-located with local decreases in bankfull width. During dam removal, a pulse of sediment temporarily filled in the pools and increased the overall sediment transport capacity of the river, but eventually most of the pools reemerged at their prior location, suggesting that width imposes an important local control on bed morphology and riffle-pool dynamics.

## ACKNOWLEDGEMENTS

I would like to thank Tim Randle and Jennifer Bountry at the United States Bureau of Reclamation in Denver for their assistance and willingness to provide data sets and their developed HEC-RAS model for the Elwha River. I also want to acknowledge fellow graduate student Jacob Morgan for his countless hours of help in the laboratory with conducting flume experiments.

## TABLE OF CONTENTS

ABSTRACT .....	ii
ACKNOWLEDGEMENTS .....	iv
INTRODUCTION.....	1
Characteristics of Riffle-Pool Sequences.....	1
Dam Removal and Morphological Response .....	5
Reservoir Sediment Sorting and Evacuation Dynamics during Dam Removal .....	10
Motivational Questions and Hypotheses .....	14
METHODOLOGY.....	15
Elwha River Dam Removal Project.....	15
Elwha Bed Surveys .....	17
Bankfull Width Mapping .....	19
Hydrologic Analysis.....	19
Numerical Modeling.....	20
Modeling Parameters.....	21
Flume Experiments .....	27
Data Measurement Techniques.....	28
Initial Conditions .....	32
Run 1: Equilibrium Conditions .....	32
Run 2: Dam Installation .....	34
Run 3: Dam Removal: Constant Sediment Feed Rate .....	34
Run 4: Dam Installation #2 .....	35
Run 5: Dam Removal #2: Sediment Pulse.....	35
RESULTS.....	37
Elwha Observations and Analysis .....	37
Sequential Pool Filling and Evacuation on the Elwha .....	37
Hydrologic Regime During Dam Removal .....	39
Bed Evolution and Width Observations .....	41
Experimental Results.....	43
Bedload Transport Results.....	43
Topography and Grain Distributions.....	44
Pulse Dynamics .....	57
Riffle-Pool Morphology and Channel Width.....	60
Pulse Dynamics .....	61
Discrepancies between the field and flume experiments .....	66
REFERENCES.....	71

APPENDIX A.....	77
Nays Numerical Validation – Bittner et al. (1995).....	77
APPENDIX B.....	79
APPENDIX C.....	81

LIST OF TABLES

**Table 1:** Summary of hydraulic and sediment transport characteristics modeled in Nays2D .....27

**Table 2:** Summary of Calculated and Modeled Equilibrium Feed Rate .....33

**Table 3:** Comparison of experimental conditions from pulse flume studies with added feed .....64

**Table 4:** Comparison of experimental conditions from 5 runs by Sklar et al. (2009).....65

**Table 5:** Comparison of experimental conditions from Run 5 of this flume study .....65

LIST OF FIGURES

**Figure 1:** Layout of a typical riffle-pool sequence and backwater profile [Knighton, 1998]. 2

**Figure 2:** Locations of riffle persistence indicated by horizontal bars in locations of greatest valley width indicated by downward arrows along with slope-subtracted bed elevation plots from 1999 and 2006 on the Yuba River [White et al., 2010]..... 3

**Figure 3:** Conceptual scale depicting Lane’s Balance, a qualitative river response model..... 8

**Figure 4:** Typical spatial distribution of reservoir sediment as observed in former Lake Mills before dam removal [Bountry, 2014]. .....11

**Figure 5:** Translation and dispersion pulse distinction [Sklar et al., 2009]. .....13

**Figure 6:** Map of the Elwha River Watershed located on the Olympic Peninsula in Washington State [The Elwha Watershed, 2014]. .....16

**Figure 7:** Elwha study reach between river stations 50+000 – 53+000 between dams. ....18

**Figure 8:** Designed flume geometry modeled with Nays2D.....21

**Figure 9:** Grain size distribution of Concrete Sand .....22

**Figure 10:** Shear Stress vs. Depth plot for multiple channel bed slope designs.....25

**Figure 11:** Shear Stress vs. Discharge plot for multiple channel bed slope designs.....26

**Figure 12:** Image of the flume with sinusoidal walls installed, inducing width variability..28

**Figure 13:** Example photo series of the image distortion correction and laser pixel extraction process.....30

**Figure 14:** Sediment surface sampling locations along the flume.....31

**Figure 15:** July 2011 channel bed and water surface profiles of the study reach before dam removal.....37

**Figure 16:** May 2013 channel bed and water surface profiles of the study reach during dam removal depicting temporary pool filling.....38

**Figure 17:** August 2013 channel bed and water surface profiles of the study reach showing pool evacuation.....39

**Figure 18:** Hydrologic Record of the Elwha during the dam removal time period at: USGS 12045500 ELWHA RIVER AT MCDONALD BR NEAR PORT ANGELES, WA.....40

**Figure 19:** Coupling of bankfull channel width from Google Earth and bathymetry from in the Elwha Study Reach. ....42

**Figure 20:** Time series of water surface profiles showing the disappearance and reemergence of a backwater profile in the Elwha study reach.....42

**Figure 21:** Bedload transport rates at the flume outlet across all five experimental runs. Vertical lines indicate the start/end of Runs 1-5. ....43

**Figure 22:** Measured water surface and bed elevations of baseline riffle-pool morphology. ....44

**Figure 23:** Digital Elevation Model of flume bed topography at baseline riffle-pool conditions (Run 1).....45

<b>Figure 24:</b> Average slope differentiated flume bed topography at baseline conditions showing established riffle-pool morphology (Run 1).	45
<b>Figure 25:</b> Grain size distributions of surface sampled riffles, pools and transitional reaches compared to the original grain distribution showing overall bed armoring (Run 2).	46
<b>Figure 26:</b> Time series of long profiles showing a base level drop and slope decrease over 24 hours of no sediment supply (Run 2).	47
<b>Figure 27:</b> Measured water surface and bed elevations of first zero supply condition.	48
<b>Figure 28:</b> Digital Elevation Model of flume bed topography at first zero supply equilibrium condition (Run 2).	49
<b>Figure 29:</b> Average slope differentiated flume bed topography at zero supply equilibrium condition (Run 2).	49
<b>Figure 30:</b> Time series of median elevation long profiles showing uniform aggradation across all riffles and pools along with a slope increase after supply was returned (Run 3).	50
<b>Figure 31:</b> Time series of flume bed topography DEM's subtracted from the baseline zero supply elevations at equilibrium after Run 2.	51
<b>Figure 32:</b> Comparison of the no feed long profiles from Runs 2 and 4 to confirm similar baseline conditions preceding dam removal experiments.	52
<b>Figure 33:</b> Digital Elevation Model of flume bed topography at second zero supply equilibrium condition.	53
<b>Figure 34:</b> Average slope differentiated flume bed topography at second zero supply equilibrium condition	53
<b>Figure 35:</b> Time series of long profiles during introduced sediment pulse showing a dramatic upstream steepening of the bed slope.	54
<b>Figure 36:</b> Time series of long profiles after sediment pulse has been fully supplied showing a relaxation of the bed slope (Run 5).	55
<b>Figure 37:</b> Time series of flume bed topography DEM's subtracted from the final topography in Run 4.	56
<b>Figure 38:</b> Downstream location of the sediment pulse front through time. The dashed line indicates when upstream feed was terminated.	57
<b>Figure 39:</b> Time series of long profiles during the pulse experiment differentiated from the baseline condition in Run 4.	58
<b>Figure 40:</b> Time series of long profiles differentiated cumulatively from the armored condition at the end of Run 4.	59
<b>Figure 41:</b> Comparison of measured bed and water surface profiles by Bittner et al. (1995) to those modeled in Nays2D.	77
<b>Figure 42:</b> Comparison of measured riffle cross sectional deformation by Bittner et al. (1995) to that modeled in Nays2D.	77
<b>Figure 43:</b> Comparison of measured pool cross sectional deformation by Bittner et al. (1995) to that modeled in Nays2D.	78

<b>Figure 44:</b> Surface material at riffle location after Run 1 (13 hours). .....	81
<b>Figure 45:</b> Surface material at riffle location after Run 2 (24.13 hours). .....	82
<b>Figure 46:</b> Location of fine sediment pulse front after 10 minutes (Run 5). .....	83
<b>Figure 47:</b> Location of sediment pulse after 27 minute (Run 5). .....	84
<b>Figure 48:</b> Sediment pulse front after 47 minutes (Run 5). .....	85
<b>Figure 49:</b> Sediment Pulse after reaching the flume outlet at 86 minutes. ....	86
<b>Figure 50:</b> Return to an armored condition after 711 minutes (Run 5). .....	87

## INTRODUCTION

### **Characteristics of Riffle-Pool Sequences**

Alternating patterns of deep, slow moving, areas (pools) and shallow, fast moving zones (riffles) are characteristic of both straight and meandering channels with heterogeneous bed material composed of small gravels to large cobbles (2-256 mm) [Knighton, 1998]. During normal flow conditions, this riffle-pool topography creates natural backwater effects (Figure 1). Riffle-pool sequences have been observed to develop freely at a regular uniform longitudinal spacing of approximately 5 to 7 bankfull channel widths in many geophysical settings [Leopold et al., 1964; Keller and Melhorn, 1978]. This riffle spacing has also been linked to naturally assumed planform characteristics. Field analysis of freely developed planform geometry has shown that a series of two riffles in an equivalent straight channel occurs at a distance of approximately  $4\pi$  channel widths [Hey, 1976; Thorne, 1997]. This value is similar to the coefficient of a stable meander wavelength developed by Richards (1982) from compiled field data.

Field observations have also presented the idea that there are consistent differences in characteristic channel width between riffle and pool features. Riffle features have been demonstrated to be consistently wider than pools in a field setting [Richards, 1976; Montgomery and Buffington, 1997]. Other work by Hey and Thorne (1986) analyzing channel width variations in gravel-bed rivers supports this too; their regression equations display consistent linear deviations in width across riffles, pools, and meander bends with riffles being the widest and pools being the most constricted [Soar and Thorne, 2001].

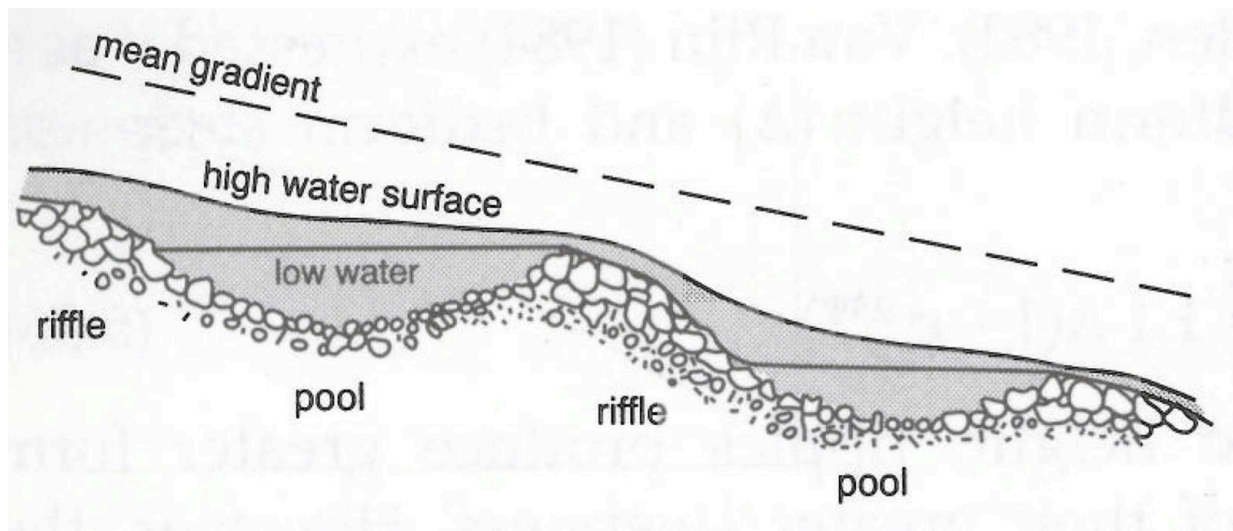


**Figure 1:** Layout of a typical riffle-pool sequence and backwater profile [Knighton, 1998].

In laterally unconfined valleys, riffle-pool sequences form freely and pools exhibit a consistent spacing of 5 to 7 bankfull channel widths. These observations were first made by Leopold and Wolman (1957) when examining the channel patterns of nearly 300 streams in a variety of geophysical settings. Additional work by Keller and Melhorn (1978) found this rhythmic spacing to naturally occur as well in both bedrock and alluvial stream channels. These findings suggesting that the development of oscillating riffle-pool topography is an important energy dissipation mechanism utilized by the fluvial system [Lisle, 1982].

However, in certain environments valley confinement has been shown to offer an important control on where riffle-pool sequences develop and persist. Work performed by White et al. (2010) examined a rapidly incising, laterally confined reach on the Yuba River in California. For this river segment, 7 persisting riffle crest locations were mapped out using aerial photo sets dating back to as early as 1937. Using longitudinal profiles and delineated valley width, the geomorphic evolution of this reach both laterally and

topographically was analyzed in great detail. Figure 2a illustrates how valley width acts as a control on the persistence of riffles in many locations of greatest valley width. Figures 2b and 2c show valley width imposing a long term control on the bed morphology as well. Slope adjusted long profiles of the reach from 1999 and 2006 show concurrent locations of riffles and pools over the 6 km reach. Despite trends of rapid incision in this system, the riffles persist in locations of greatest width through time [White et al., 2010].

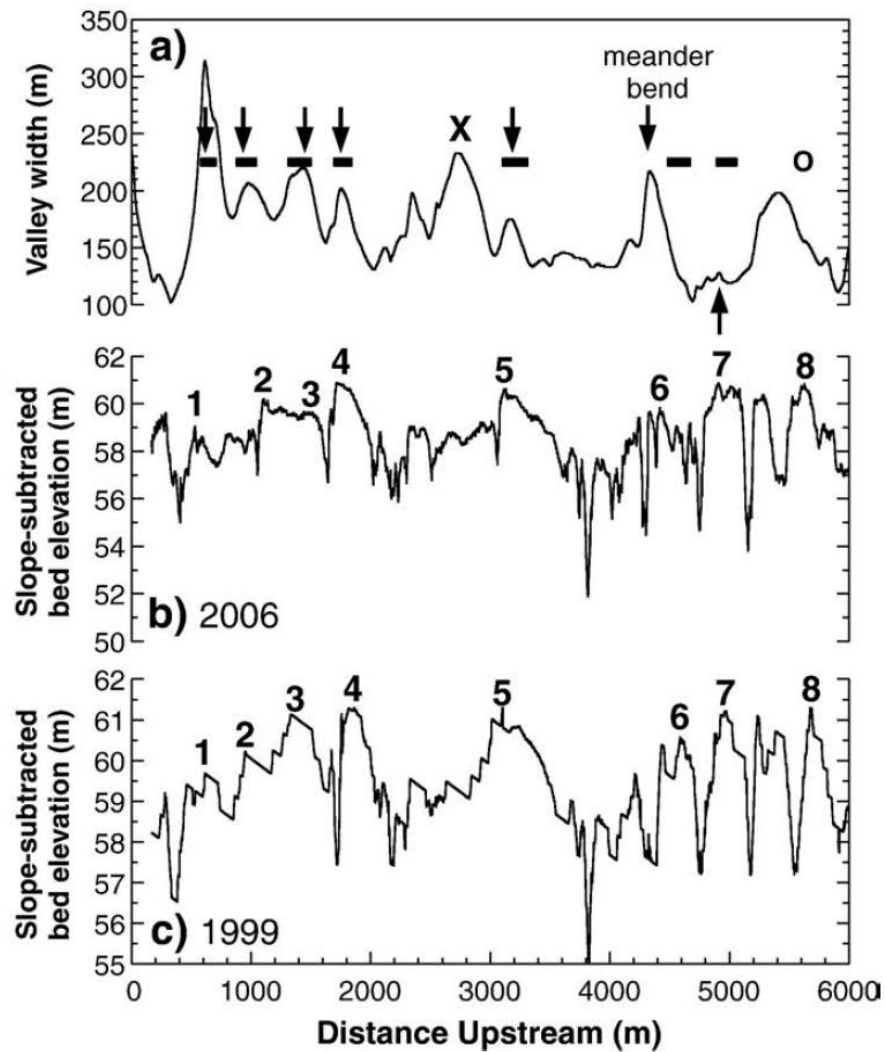


**Figure 2:** Locations of riffle persistence indicated by horizontal bars in locations of greatest valley width indicated by downward arrows along with slope-subtracted bed elevation plots from 1999 and 2006 on the Yuba River [White et al., 2010].

Local controls have been demonstrated to override valley characteristics and dictate where pools form, otherwise known as forced riffle-pool systems. Channels with high wood loading have been shown to exhibit more frequent pool spacing [Montgomery et al., 1995]. Obstructions such as boulders and large woody debris (LWD) create flow convergence, additional turbulence, and increased sediment transport capacity that leads to scour of the channel bed and pool development [Swanson et al., 1976; Keller and Swanson, 1979; Lisle 1986; Montgomery and Buffington 1997]. These roughness elements have been identified as the primary driver of pool development in many coarse-grained, mountain rivers [Buffington et al., 2002].

Work by de Almeida and Rodriguez [2012] with one-dimensional morphodynamic modeling has shown that in addition to channel width, variable discharge can influence the spontaneous formation of riffle-pool sequences. By comparing simulations of steady and unsteady hydrographs, the unsteady hydrology produced more quasi-natural riffle-pool relief. Steady flow at higher discharges did produce similar relief in a variable width setting. These results show certain thresholds of flow magnitude are needed to develop riffle-pool relief and maintain its morphology.

A theory as to how pool features are maintained throughout the natural flow regime was first put forth by E.A. Keller (1971), known as the hypothesis of velocity reversal. This hypothesis suggests that at more frequent lower magnitude discharges, the velocity in a riffle is greater than that of its corresponding pool and finer materials are transported out the riffle and deposited in the neighboring pool. However, at higher channel forming discharges the bottom velocity in a pool exceeds that of the adjacent riffle and these finer deposits are scoured from the pool bottom and deposited in the downstream riffle.

Additional work with comprehensive 2-D and 3-D hydraulic modeling has introduced the concept of flow convergence due to channel width variability as the primary driver of riffle-pool maintenance [Thompson et al., 1996; Thompson et al. 1999; MacWilliams et al., 2006; Thompson and Wohl 2009]. A high velocity jet in the pools center coupled with a recirculating eddy region causes scour induced by converging flow entering the pool and diverging flow exiting. The modeling work done by de Almeida and Rodríguez [2011] provides additional insights on the role of a natural hydrograph and sediment variability on riffle-pool maintenance. Their findings show that grain size sorting can under certain circumstances lead to a sediment transport reversal (i.e., sediment transport in the pool becomes greater than that over the riffle) before velocity reversal occurs.

The development and maintenance of riffle-pool relief is important to aquatic ecology and overall stream health. Riffle features are shallow, high velocity zones in the natural setting and thus provide cool, well oxygenated water that is important during periods of warmer stream temperature [Ewing, 2013]. Because of these high concentrations of dissolved oxygen, many aquatic macroinvertebrates grow to maturity in these locations. As nymphs are dislodged from rocks into the flow, a steady “biological drift” is provided to predators downstream; making these areas critical feeding habitat [Allan & Castillo, 1995]. In contrast, pools provide deep, slow moving water that protects fish from predation and creates a refuge that requires minimal energy expenditure.

### **Dam Removal and Morphological Response**

Dam removal is becoming a common practice to restore fluvial, morphodynamic, and ecological function to river systems. It is estimated that 1,150 water impoundment and diversion structures have been removed in the United States since 1912 [American

Rivers, 2014]. The removal of 850 or 74% of these structures has occurred within the last two decades [American Rivers, 2014]. Removing a dam is important to restoring the river's natural flow regime, providing connectivity, and reintroducing additional sediment supply. In coastal regions dams are very detrimental to the survival rate of anadromous fish species attempting to migrate upstream and complete their life history. In many cases these dams have limited uses today as their structural integrity is of concern and have become inefficient sources of hydropower [American Rivers, 2014]. In other situations where expensive fish passage structures have been mandated, it may be more economically feasible to remove the dam entirely. With this in mind, certain precautions must be taken when removing a dam as it has likely trapped large quantities of sediment over its lifespan.

The evacuation process of this reservoir sediment should not be overlooked as it may lead to extremely detrimental downstream ramifications during a dam removal project. These high sediment loads have the potential to negatively impact water quality, aquatic habitat and infrastructure. Both the quantity and quality of reservoir sediments can be problematic with a dam removal. High levels of fine sediment in suspension can cause short-term fish kills and harm populations of other aquatic organisms. Contaminants that have settled out in reservoirs and leached into sediments may be remobilized during dam removal and negatively impact water quality [The Heinz Center, 2002]. The transport of high sediment loads will alter the river's morphology and may have negative impact on aquatic habitat in the short-term. Some consequences may include the reduction of desirable backwater features or fine sediment carpeting larger spawning gravels necessary for salmon reproduction [The Heinz Center, 2002]. Finally,

turbidity from suspended sediment has the potential to impact water treatment infrastructure downstream. Suspended sediment has damaged the Water Treatment Plant for the city of Port Angeles by the Elwha Dam Removal and resulted in costly repairs [Schwartz, 2013]. Therefore, a well-developed fundamental understanding of how increased sediment supply propagates through and interacts with a riffle-pool system below a dam site is desired.

E. W. Lane (1955) developed a well-regarded qualitative response model to explain how a fluvial system will likely respond to alterations in available water or sediment with a conceptual scale (Figure 3) known as “Lane’s Balance”. This proportionality relationship is based around a dynamic equilibrium of water and sediment represented in the following equation:

$$Q_s D_{50} \propto QS \quad \text{Eq. 1}$$

$Q_s$  is defined as the total sediment load transported,  $D_{50}$  the median grain size of the sediment load,  $Q$  the discharge of the river and  $S$  being the local channel slope.

Similarly, Schumm (1977) built upon this idea with a River Metamorphosis concept that introduced additional morphological variables. His model introduced both cross sectional and planform characteristics that were not included in Lane’s model. Of particular interest are the scenarios dealing with alterations of sediment load and grain size as shown below:

$$Q_s^- D_{50}^+ \propto S^-, b^-, d^+, \lambda^-, P^+ \quad \text{Eq. 2}$$

$$Q_s^+ D_{50}^- \propto S^+, b^+, d^-, \lambda^+, P^- \quad \text{Eq. 3}$$

In Eq. 2 and Eq. 3,  $Q_s$  is defined as the total supplied sediment load and  $D_{50}$  the median grain size of that supply. Variables defining channel geometry are the local channel slope  $S$ , the channel width  $b$ , and the cross sectional depth  $d$ . River planform characteristics are integrated as well through the inclusion of the meander wavelength  $\lambda$  and sinuosity  $P$ .

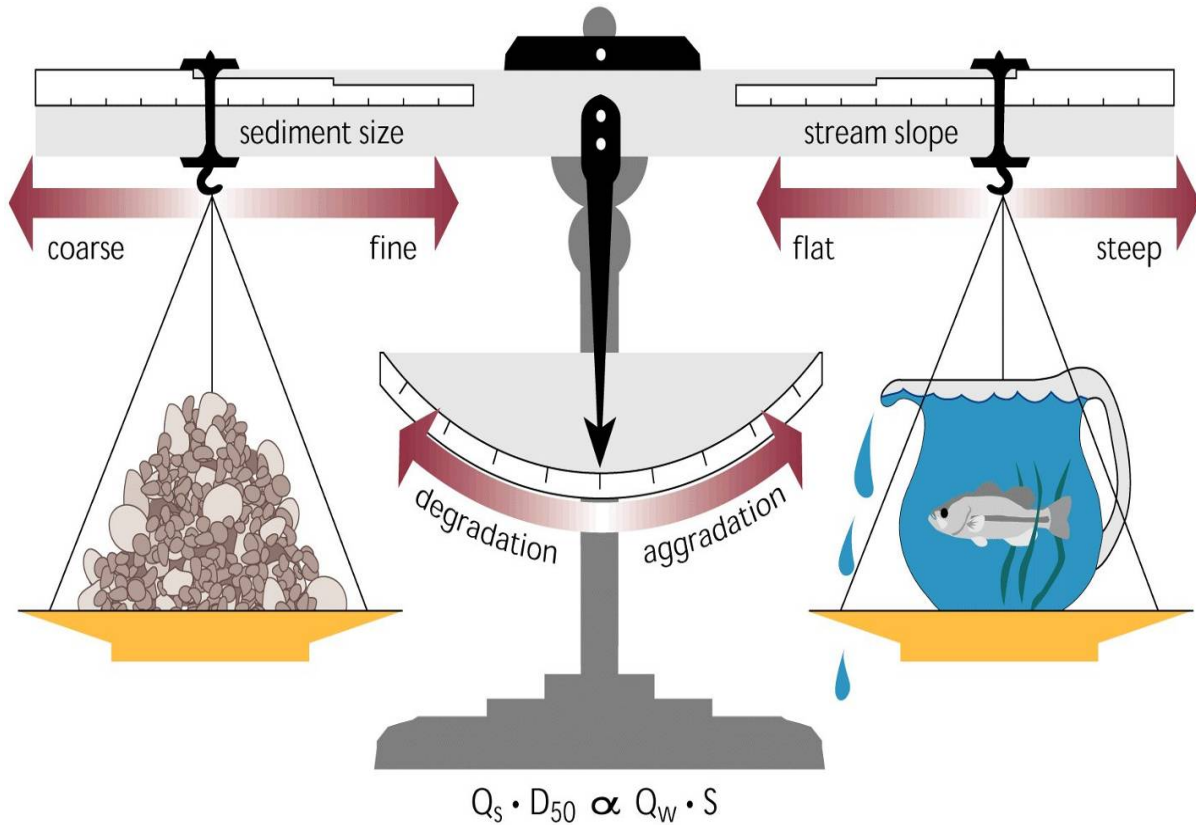


**Figure 3:** Conceptual scale depicting Lane's Balance, a qualitative river response model

This model suggests that when a dam is installed in a dynamically equilibrated river, the system will respond to a large decrease in sediment delivery composed of

coarser material by altering its bed slope while going through an initial period of incision and narrowing below the dam due to excess transport capacity. Planform characteristics are expected to adjust as well with a reduction in the meander wavelength and a more sinuous channel. Decades or centuries later when the dam is decommissioned and removed, reservoir sediments are mobilized; both an increase in sediment delivery downstream and a decrease in the median grain size of bedload transport should then be expected to occur. Schumm's model would characterize the geomorphic response to be net aggradation on the channel bed and a steepening of the channel bed slope. Planform adjustments should create a more frequently meandering, more energetic, less sinuous river. These conceptual models are useful in predicting a fluvial system's response tendencies, however what might occur when the supply is of large magnitude, episodic, and uniform in grain size?

Quantitative observations have been made through laboratory experiments and numerical modeling that validate Schumm's River Metamorphosis ideas. Experiments by Nelson et al. [2009] show an increase in the surface  $D_{50}$  with time as the sediment feed rate was reduced. Water surface and bed slope exhibited downward trends with reductions in supply as qualitatively described in Equation 2. These trends aligned with numerical predictions made solving the Parker (1990) and Wilcock and Crowe (2003) sediment transport models with the 1-D Exner equation [Nelson et al. 2009]. Physical modeling performed by Venditti et al. (2012) examined alternate bar response to supply termination. Similar results were shown with the cessation of sediment supply; an increase in grain size and a relaxation of the bed slope were observed as the alternate bar

features disappeared. When supply was restored, the system responded through fining of the bed surface and steepening of its slope as described in Eq. 3, while reestablishing bars.

### **Reservoir Sediment Sorting and Evacuation Dynamics during Dam Removal**

Both field observations and physical models of dam removal scenarios describe the reservoir material prograding coupled with a channel rapidly incising through the deposits. The sediments transported below the dam site tend to sort vertically as they slide down the delta front [Cantelli et. al, 2004]. During this process, the fine sediments that have settled out below the reservoir are brought into suspension and transported past the dam site before the coarser sands, gravels, and cobbles (Figure 4). Observations of large scale dam removals such as the series of two dams on the Elwha River describe this sequential grain sorting phenomenon [Bountry, 2014]. The Elwha watershed is a coastal system, so dam removal resulted in an immediate reformation of an estuarial beach at the Strait of Juan de Fuca composed of silty material. It is expected that coarser material in the former reservoir deposits will be evacuated sequentially by grain size with fluctuations in the hydrologic regime over the next several decades [Bountry, 2014]. With this in mind, it is important to consider the importance of the well sorted nature of these sediment releases when attempting to mimic a phase of the dam removal process.

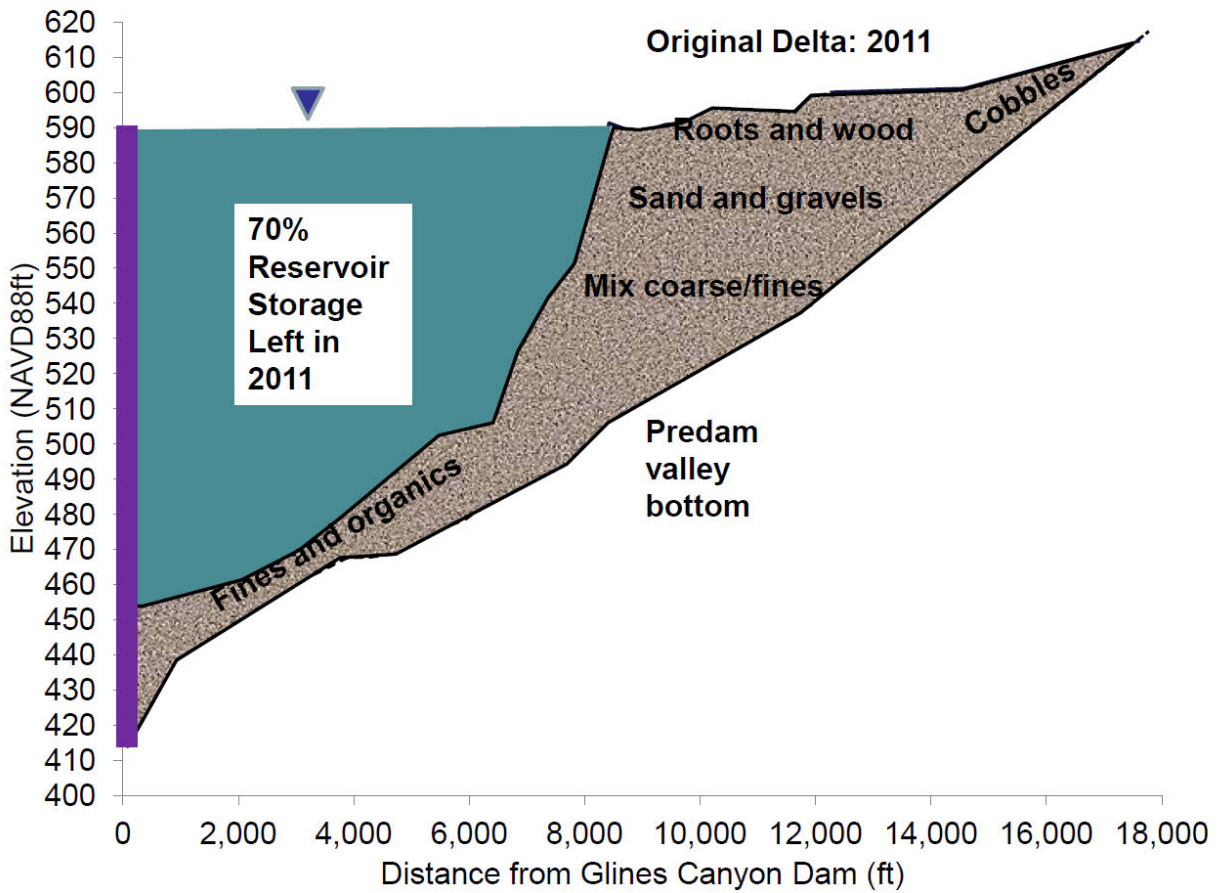


**Figure 4:** Typical spatial distribution of reservoir sediment as observed in former Lake Mills before dam removal [Bountry, 2014].

Experiments and observations have also demonstrated a pulse like phenomenon as to how the sediment is evacuated below the dam site during removal [Cui et al., 2008; Bountry, 2014]. This evacuation process appears to be analogous to natural pulses introduced by landslides and debris flows in Mountain Rivers and has been modeled as such [Cui et. al, 2003b]. The magnitude of the pulse can be altered by the mechanism through which the dam is removed. An incremental removal process was used on the Elwha River in an attempt to offer a more controlled sediment release and limit the magnitude and turbidity of pulse flows [Bountry, 2014]. This suggests that the dynamics

of sediment releases on the Elwha in particular may exhibit similarities to gravel augmentation pulses, a common restoration practice.

The relative translation and dispersion of a gravel augmentation pulse will determine how long that added gravel remains in the channel and may affect restoration planning and operation [Sklar et al., 2009]. How translational and dispersive a sediment pulse is can be expressed through downstream profiles of pulse thickness (i.e., difference in elevation from baseline, pre-pulse conditions) and downstream profiles of the cumulative elevation difference (Figure 5). Sklar et al. (2009) performed experiments in a straight rectangular flume and showed that pulses display both translation and dispersion, with a significant translational component. In their experiments, five distinct sediment pulses were introduced with five distinct grain size distributions as well as two magnitudes. Translation was more evident in the pulses of smaller mass, and these finer grained distributions moved through the system in a shorter period of time.

Other experiments conducted by Lisle et al. (1997) demonstrated that introducing a central sediment wave into a channel that has developed an alternate bar morphology will lead to a dispersion-dominated response with the bar morphology remaining intact. Work by Cui et al. (2003a) offered additional insights into sediment pulse propagation by designing several experimental pulses with varying grain sizes. Findings from three runs show that sediment pulses are primarily dispersive but may evolve more rapidly and have translational characteristics when composed of material finer relative to the preexisting substrate. In contrast to Lisle et al. (1997), Cui et al. (2003a) present the idea that previously developed topography can be temporarily obliterated by a sediment pulse and reemerge with time. Results from these experiments contradict findings by Benda and

Dunne (1997a and 1997b) that suggest naturally occurring pulses primarily translate through a channel network with little dispersion. Their analysis was performed at a watershed scale and used to develop a numerical model. Overall, results on the topic of sediment pulses suggest that the development of bed morphology plays an important role in how a channel responds to an increase in sediment supply, but this concept is still poorly understood in the context of width variability.

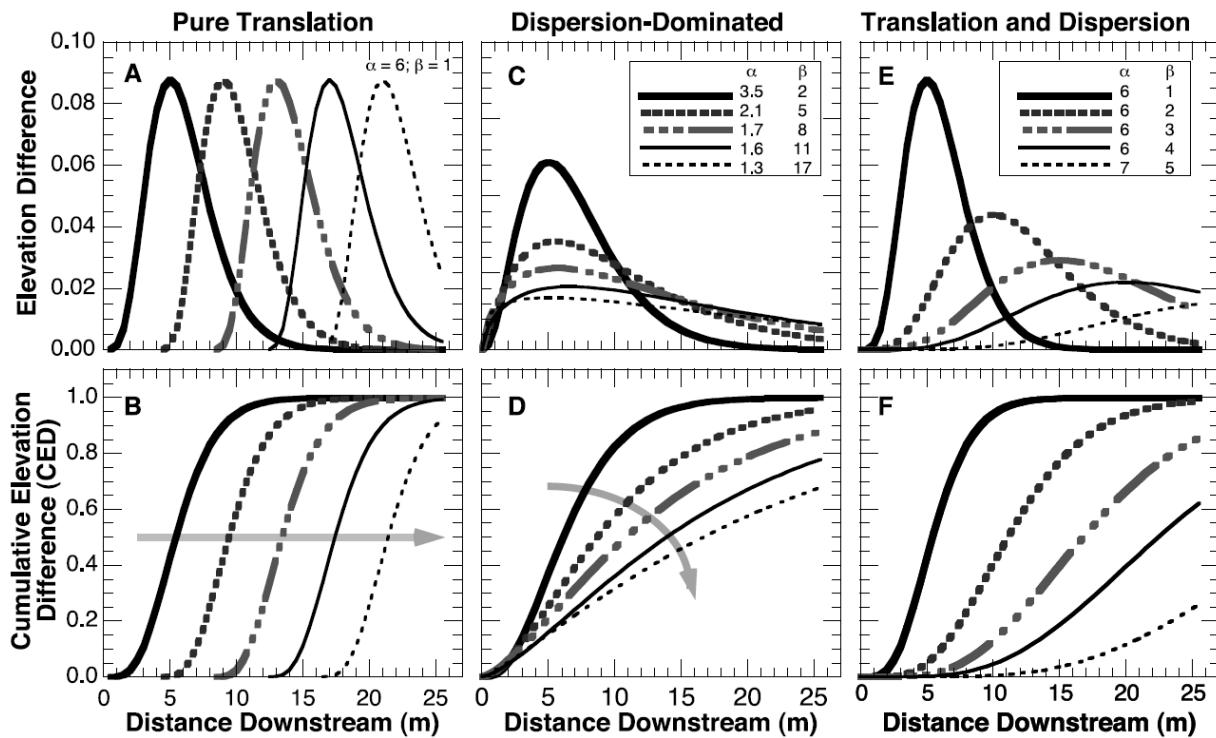


**Figure 5:** Translation and dispersion pulse distinction [Sklar et al., 2009].

## **Motivational Questions and Hypotheses**

The overall goal of this study has been to understand how variable width channels respond to changes in sediment supply. The questions we chose to address are: (a) is riffle-pool morphology in variable width channels persistent given large changes in sediment supply, (b) does a pulse of sediment behave differently than a uniform increase in sediment supply and (c) how does a pulse of sediment longitudinally propagate through a straight, variable width channel?

We hypothesized that width variations and increases in sediment supply interact dynamically to affect riffle pool morphology. Specifically, we expect (a) with a uniform supply increase, the channel will increase in slope but maintain its riffle-pool relief; (b) with an introduced sediment pulse, the channel will preferentially fill in its pools to increase transport capacity, but in the absence of large channel forming events, width variation will cause the channel to redevelop pools at local constrictions and riffles at expansions in previous locations and (c) a sediment pulse will propagate primarily in a dispersive manner in a variable width channel with riffle-pool topography. By addressing these fundamental questions, we hope to find answers that will be useful to river scientists and managers during dam removal projects and throughout post-removal monitoring and restoration.

## METHODOLOGY

This study offers a complementary analysis of field bathymetry and aerial imagery with physical modeling. First, bathymetric geospatial data sets collected by the Bureau of Reclamation (USBR) during float surveys before and during dam removal on the Elwha River were analyzed and compared. In addition, the longitudinal pattern of bankfull channel width during the dam removal project on the Elwha was digitized using aerial imagery. These field data then motivate two-dimensional morphodynamic modeling and flume experiments conducted at the Colorado State Engineering Research Center (ERC).

### **Elwha River Dam Removal Project**

The Elwha River is located on the Olympic Peninsula in Washington State. It flows from its snow field headwaters in Olympic National Park 45 miles to the Strait of Juan de Fuca in the Pacific Ocean (Figure 6). Historically the Elwha river network has been very productive salmon system with typical annual spawning runs of 400,000 fish [Smillie, 2014]. The Elwha was once a member of a select few Pacific Northwestern rivers that supported all five Pacific salmon species (Chinook, chum, coho, pink, sockeye) in addition to four species of anadromous trout (Steelhead, coastal cutthroat, bull, and Dolly Varden char). Beginning in 1910, Elwha Dam, the first of a series of two dams, was constructed at river mile 4.9 in the lower reaches of the river. The dam was poorly constructed and subsequently failed in 1912. However the dam was rebuilt and completed by 1913. 12 miles upstream, Glines Canyon dam was built at river mile 17 below a very confined canyon reach and completed by 1926. The dams provided an economic jumpstart to the surrounding town of Port Angeles by supplying cheap hydropower to a paper mill.

However, the dams lacked fish passage, and since then it has been estimated that salmon returns have been reduced to as low as 4,000 fish annually.

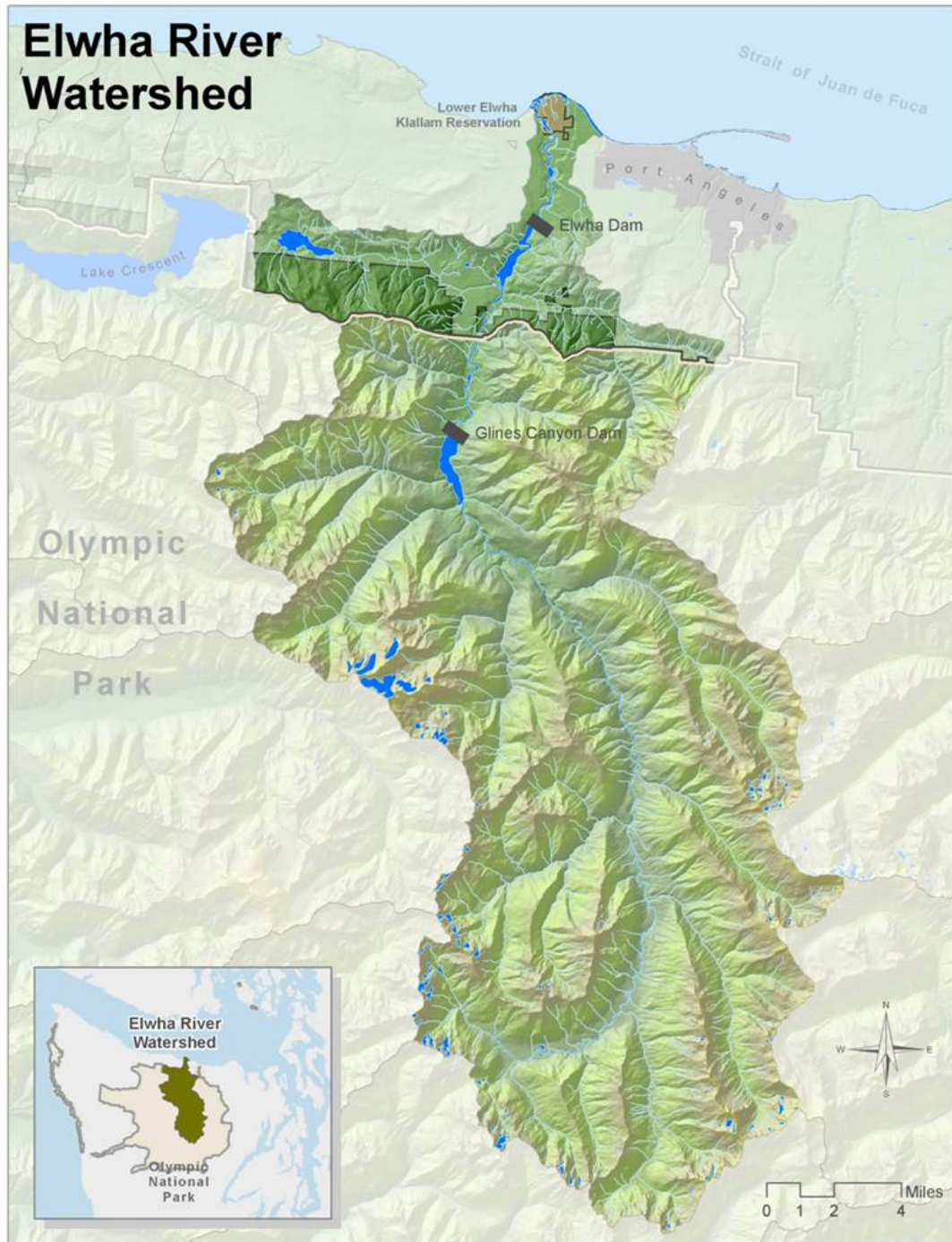


**Figure 6:** Map of the Elwha River Watershed located on the Olympic Peninsula in Washington State [The Elwha Watershed, 2014].

As decades passed it became clear that the dams were inefficient at generating power and more detrimental to the ecosystem than their benefits provided. In 1992, George H. W. Bush signed the Elwha River Ecosystem and Fisheries Restoration Act into law. This transferred ownership the dams to the federal government and allocated funds to dam mitigation. After reservoir sedimentation modeling and laboratory experiments conducted by Bromley et al. (2011), it was determined that the sedimentation issues could be managed by removing the dams in a controlled manner. An estimate from the USBR predicted that 34 million yd<sup>3</sup> of sediment had been trapped in the reservoirs with 28 million yd<sup>3</sup> of it behind Glines Canyon Dam in Lake Mills. Beginning with Elwha Dam in Fall of 2011, both dams have gone through stepped down removal and periods of holding to allow reservoir sediments to stabilize and anadromous fish to move through the Elwha main stem and into tributaries. Elwha Dam was completely removed in March of 2012 and less than 30 feet of Glines Canyon Dam remain today (as of July 2014) with scheduled completion by September 2014. Turbidity issues due to increased reservoir sediment have occurred at a downstream water treatment plant, but overall the project has gone to plan and is viewed as a major success among large-scale dam removal projects.

### **Elwha Bed Surveys**

Throughout this dam removal project, the USBR has collected bathymetric data showing the morphological evolution of the Elwha River. Data sets are available from pre-dam removal in July 2011 through their most recent survey in November 2013. Boat survey data has been refined by Jennifer Bountry to reduce the data set to points more representative of the channel thalweg. We selected a stable reach between the two dam sites from river stations 50+000 to 53+000 for a high-resolution analysis shown in Figure

7. This stationing corresponds to the distance in feet upstream from the river mouth at the Strait of Juan de Fuca, with the “+” symbol analogous to a comma. This particular site was chosen due to its low planform sinuosity, consistent bankfull channel width through time, and close proximity to the McDonald Bridge USGS gage station downstream at river station 44+371. This reach was also spaced far enough upstream that the hydrologic regime is not significantly altered from backwater effects created by Elwha Dam. Particular data sets of interest that were used in further analysis included the May 9, 2013 and August 1, 2013 bed profiles.



**Figure 7:** Elwha study reach between river stations 50+000 – 53+000 between dams.

## **Bankfull Width Mapping**

To obtain an understanding of how width might interact with riffle-pool morphology in the Elwha system, an analysis was performed on a series of aerial images available on Google Earth. Aerial photos from June 6, 2009, September 3, 2012 and July 5, 2013 were selected because they were the closest in time to the bathymetric surveys of interest. For each aerial photo, bank lines corresponding to the bankfull discharge were estimated and digitized. Indicators such as sand bars, dense vegetation and terraces were used to visually estimate this. Along with this, the channel centerline was created by estimating the current thalweg under normal flow conditions. This geometry was exported as KML data and converted to shape files in ARCGIS. The banks were used to develop a polygon containing both banks and the extents of the river reach. Cross-sections perpendicular to this centerline were created at 1-ft intervals and trimmed within the boundaries of this polygon.

## **Hydrologic Analysis**

A hydrologic analysis was performed on the Elwha during the period of dam removal using streamflow data from USGS gage 12045500 at McDonald Bridge. Both daily average values and daily maximum 15-minute instantaneous peaks were gathered over the period of interest: September 10, 2011 to present (June 28, 2014). These values were plotted with time to generate a hydrograph for the Elwha. Annual peak flow values were collected as well, with hydrologic data available beginning in 1897. These data were plotted using a common Log-Pearson Type III ranking technique from highest to lowest discharge. Next the recurrence interval of various events in the annual maximum series were calculated using Eq. 5:

$$T = \frac{R}{n+1} \quad \text{Eq. 5}$$

With  $R$  being defined as the overall rank of that discharge in the annual maximum series,  $n$  being the number of peak flow values, and  $T$  being the return period of that particular flow in years. After analyzing a dam removal project in a field setting it was important to next develop a numerical model that would guide flume experiments that would examine the influences of channel width and increased sediment supply.

### **Numerical Modeling**

Nays2D is a two-dimensional, unsteady flow model that can compute both river hydraulics and erosional processes. This numerical model was developed by Dr. Yasuyuki Shimizu of Hokkaido University in Japan. It is a build-in to iRIC (International River Interface Cooperative), which is a freely available pre- and post-processing software package for multi-dimensional hydraulic and morphodynamic modeling. The model's sediment transport capabilities include bedload, mixed suspended load, and both uniform and mixed grain size distributions. The model was used as a preliminary tool to establish initially parameters that would achieve the desired outcomes in the flume experiments. Nays2D was selected as an appropriate numerical model through a validation process (Appendix A). Variable width physical modeling experiments performed by Bittner et al. (1995) were re-created accurately using Nays2D, deeming it a suitable model to predict hydraulic conditions.

### **Modeling Parameters**

The physical model was to be performed on a straight rectangular flume, however width variability was needed to develop riffle-pool relief. We planned to install sinusoidal walls that would constrict the flow in certain locations and scour out pools. The wavelength of the walls was designed to space the constricted sections at a spacing of five riffle widths as observed in natural settings [Leopold and Wolman, 1957]. The flume has a maximum width of 21.6 cm, therefore one wavelength of the sinusoid became 1.08 m. Comparing bankfull width changes on the Elwha, a 40% reduction in width appeared to be suitable. Thus the narrowest sections would have a width of 15.4 cm, giving the sine wave an amplitude of 3.09 cm and a wavelength of 1.08 m as illustrated in Figure 11. With a total flume length of 9.14 m, it was estimated that 6 wavelengths could fit with an adequate inlet and outlet reach. This preliminary geometry and selected bed slope was integrated into a MATLAB script that generated a *.riv* topography file that would be imported into Nays2D.

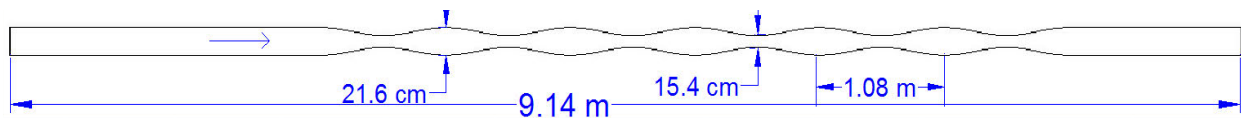


**Figure 8:** Designed flume geometry modeled with Nays2D

The sediment grain size distribution of the mobile bed and upstream supply was selected based on available sand from a local materials distributor (Martin Marietta, Fort Collins, CO). It was decided that a premixed Concrete Sand, primarily consisting of sand and a small fraction of fine gravel would be used (Figure 9). The median grain diameter or  $D_{50}$  is 0.85 mm, scaling roughly 1:250 with the median grain size of a typical gravel bed river such as the Elwha. This value was used for sediment transport calculations in the

hydraulic design. Calculations were performed to design the equilibrium flow depth so that sediment transport would occur as bedload only while maintaining an adequate width to depth ratio.

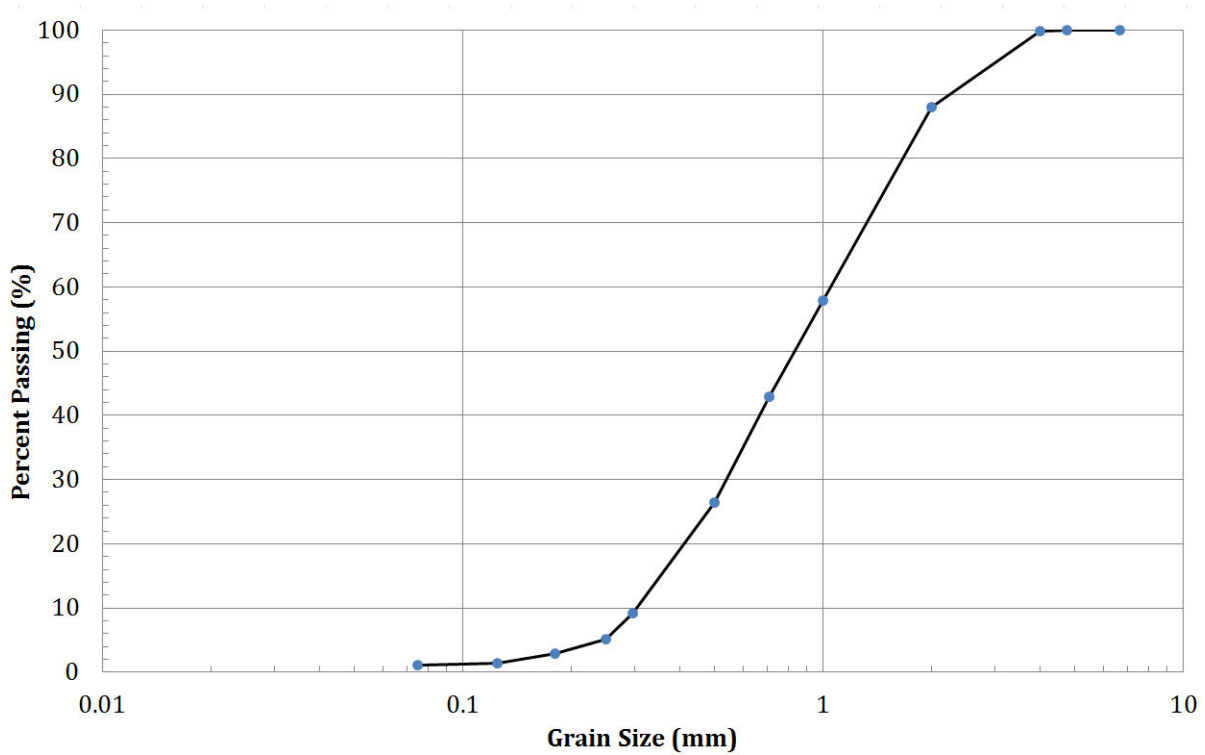


**Figure 9:** Grain size distribution of Concrete Sand

The modified Shields diagram was utilized to determine the lower bound of particle mobility. Interpreting the modified Shields diagram where shear velocity has been removed, a critical shear stress value ( $\tau_{*c}$ ) for the median particle size  $D_{50}$ , was estimated to be 0.03 based on a dimensionless particle ( $d_*$ ) value of 20.56, calculated using Eq. 6 [Julien, 2010]. The parameter  $g$  is defined as the gravitational constant,  $G$  is the specific gravity of sediment (assumed to be 2.65), and  $\nu$  is the viscosity of clear water.

$$d^* = D_{50} \left[ \frac{(G-1)g}{v^2} \right]^{1/3} \quad \text{Eq. 6}$$

This value was then inserted into the general shear stress equation and doubled (0.06) to ensure mobility beyond incipient motion ( $\tau_{min}$ ), shown in the equation below [Shields, 1936]:

$$\tau_{min} = 2\tau_{*c}D_{50}g(G-1) \quad \text{Eq. 7}$$

To calculate the upper shear stress limit, the fall velocity for the median particle size was calculated based on a general fall velocity equation for particles in clear water [Julien, 2010].  $C_D$  is the coefficient of drag forces based on a grain particles size and shape and fall velocity ( $\omega$ ) is the velocity at which drag and buoyant forces on a particle are equal to downward gravitational forces:

$$\omega = \left[ \frac{4}{3} (G-1) \frac{gD_{50}}{C_D} \right]^{1/2} \quad \text{Eq. 8}$$

The ratio of a particle's shear velocity ( $u^*$ ) or submerged velocity due to fluid shear forces to fall velocity ( $\omega$ ) will determine its mode of transport. If this ratio is greater than 0.2 and less than 0.5, bedload is the primary mode of transport [Julien, 2010]. To determine the upper bound of shear stress for bedload transport the resultant fall velocity value of 0.11 m/s was divided by 2 to calculate a shear velocity that maintains this ratio. It was then

inserted into the shear velocity equation rearranged for shear stress below, to determine the upper limit with ( $\rho$ ) defined as the density of water:

$$\tau_{max} = \rho u_*^2 \quad \text{Eq. 9}$$

This defined an allowable range in shear stress between 0.79 and 3.30 pascals. To calculate the design discharge, hydraulic continuity and the Chezy relation (Eq. 11) were iteratively solved for a range of discharges ( $Q$ ) and slopes ( $S$ ), with  $R$  being the hydraulic radius or area of a riffle cross section divided by its wetted perimeter. The constant  $C$  is a classic logarithmic roughness profile [Einstein, 1950]. Another design constraint was that the width ( $w$ ) to depth ( $h$ ) ratio should be close to a value of 15 in the riffles and that was incorporated when selecting a depth and discharge. These equations are shown below rearranged to both solve for velocity ( $v$ ):

$$v = \frac{Q}{hw} \quad \text{Eq. 10}$$

$$v = C\sqrt{gRS} \quad C = 6 + 2.5 \ln\left(\frac{h}{2.5D_{50}}\right) \quad \text{Eq. 11 and 12}$$

The preferred initial slope was selected to be 0.007 because it both matched the Elwha prototype and minimized the flow rate necessary to exceed the shear stress threshold.

A plot of discharge vs. depth below shows multiple design slopes and the dashed line represents the depth of 1.44 cm needed to match the designed width to depth ratio (Figure

10). Thus, the depth was rounded to 1.5 cm for practicality, maintaining a width to depth ratio of 14.4 in the widest sections.

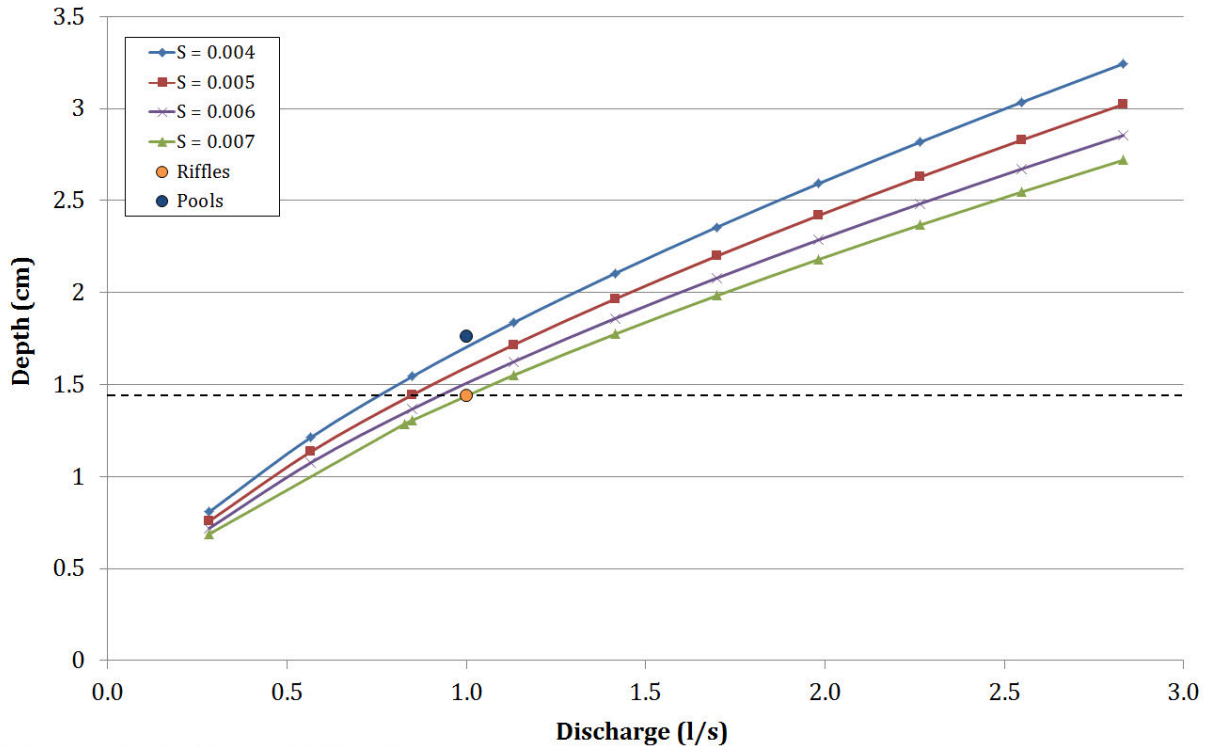


**Figure 10:** Shear Stress vs. Depth plot for multiple channel bed slope designs.

At this slope, a discharge of at least 0.83 l/s was needed to exceed the shear stress required for sediment transport in the wider flume sections as shown in Figure 11.

A value of 1 l/s was decided upon for practicality, which should equate to an average flow depth of 1.5 cm at the downstream outlet with equilibrium conditions.

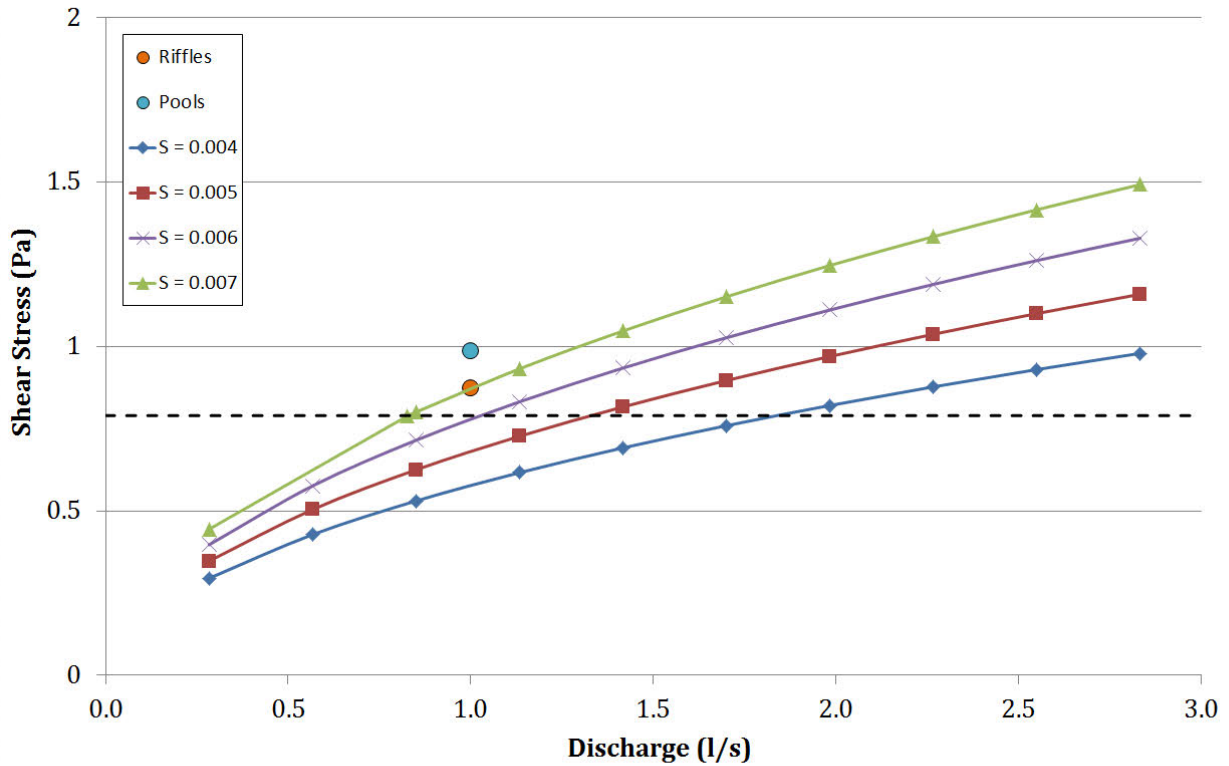


**Figure 11:** Shear Stress vs. Discharge plot for multiple channel bed slope designs.

Once the initial flume topography was imported, a boundary fitted calculation mesh composed of 470 downstream and 20 cross-stream grid cells (producing a characteristic cell spacing of 4 cm in the downstream direction, cell size was variable in the cross-stream direction based on channel width with cells being 2.7 cm in the widest sections and 1.2 cm in the most constricted locations) was generated within iRIC. In the Nays2D simulation, the water discharge was a constant 1 l/s, Manning's n was set to 0.020, and the bed material was given the gradation shown in Figure 10. Mixed-grain-size bedload transport was computed using the Ashida-Michiue (1972) formula. The model was set to run for 8 hours, with a calculation time step of 0.0005 s. For boundary conditions, the water surface elevation at the downstream end was specified to be the normal flow depth, and the sediment transport rate at the upstream end was assumed to be equal to the equilibrium

sediment transport capacity. At the end of each computational time step, the new bed elevation and bed surface grain size distribution were computed by solving the mixed-grain-size Exner equation of sediment continuity. The model did predict the formation of central pools and riffles and therefore suggested a good geometry for proceeding flume experiments. Parameters of interest such as bedload transport rate and magnitude of topographic relief between riffles and pools were of particular interest in designing the flume experiments. Table 1 shows the hydraulic and morphodynamic modeling parameters for this flume calculated in Nays2D.

**Table 1:** Summary of hydraulic and sediment transport characteristics modeled in Nays2D

Depth in riffles (cm)	1.44
Depth in pools (cm)	1.59
Discharge (l/s)	1.00
Discharge (cfs)	0.035
Boundary shear stress in pools (Pa)	0.99
Shields stress in pools	0.075
Equilibrium feed rate (m <sup>2</sup> /s)	1.3 x 10 <sup>-5</sup>
Equilibrium feed rate (grams/min)	250

## Flume Experiments

Experiments were performed on a 9.14 m x 21.6 cm x 38.1 cm (L:W:H) plexiglas flume at the Colorado State University Engineering Research Center’s hydraulics laboratory. Similar to the sediment, the flume geometrically scaled 1:250 to a gravel bed river field prototype such as the Elwha. As designed, six sets of sinusoidal walls with a wavelength of 1.08 m and amplitude of 3.09 cm were installed intermediately in the flume. A 1.58 m inlet reach was provided with several rows of ¼” diameter PVC pipes installed at

the upstream most end to act as flow straighteners, allowing uniform flow to develop entering the flume. In addition, a 1.08 m outlet was provided to limit overfall effects from propagating upstream, into the sinusoidal width sections. A head box was installed at the upstream end to provide the designed flow rate; water was supplied by a pipe from the facility's water system (Figure 12).



**Figure 12:** Image of the flume with sinusoidal walls installed, inducing width variability.

### ***Data Measurement Techniques***

The focus of this study was to understand the morphodynamic change of the flume bed; therefore a detailed and accurate methodology was adopted to properly characterize

bed evolution at a micro-topographic scale. A Canon Rebel t3i digital SLR camera was mounted to a flange onto a board the width of the flume. The camera was positioned upside-down, angled approximately 45 degrees from vertical, pointed upstream. A laser level was mounted to another flange, projecting a laser line aimed directly vertical at the bed. The camera was used to take a photograph of the laser at 2 cm intervals along the length of the flume. These photos could then be altered with a MATLAB script to correct for vertical distortion and processed into cross-sections (Figure 13).



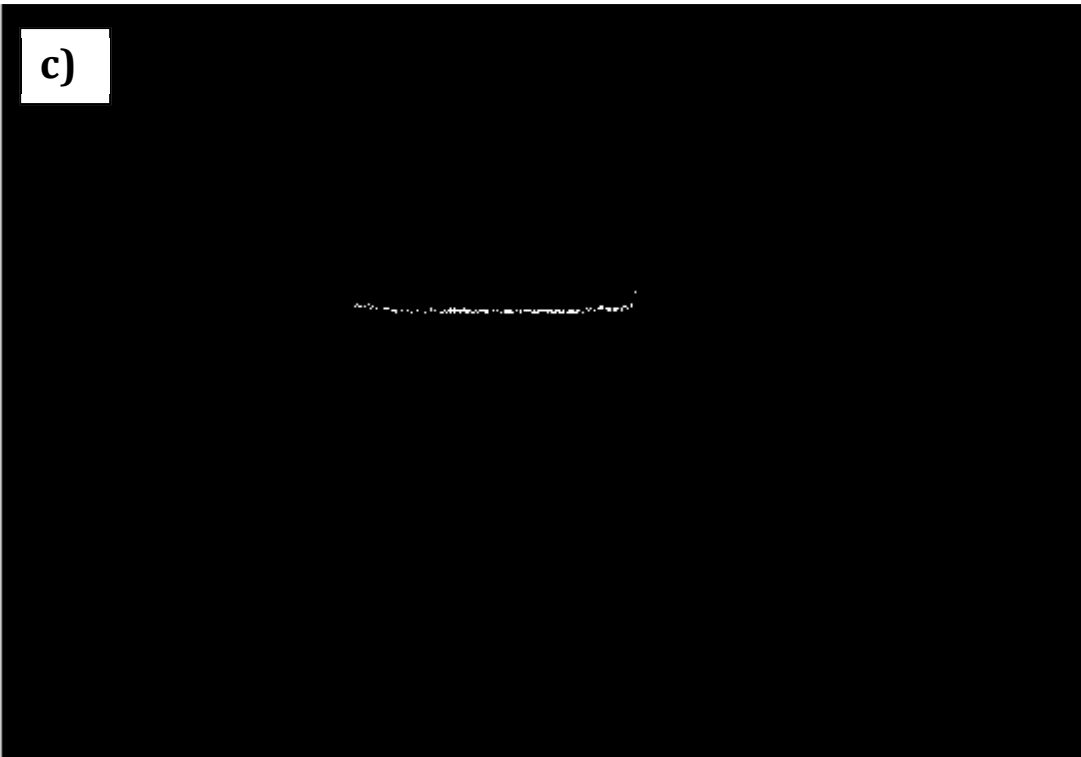
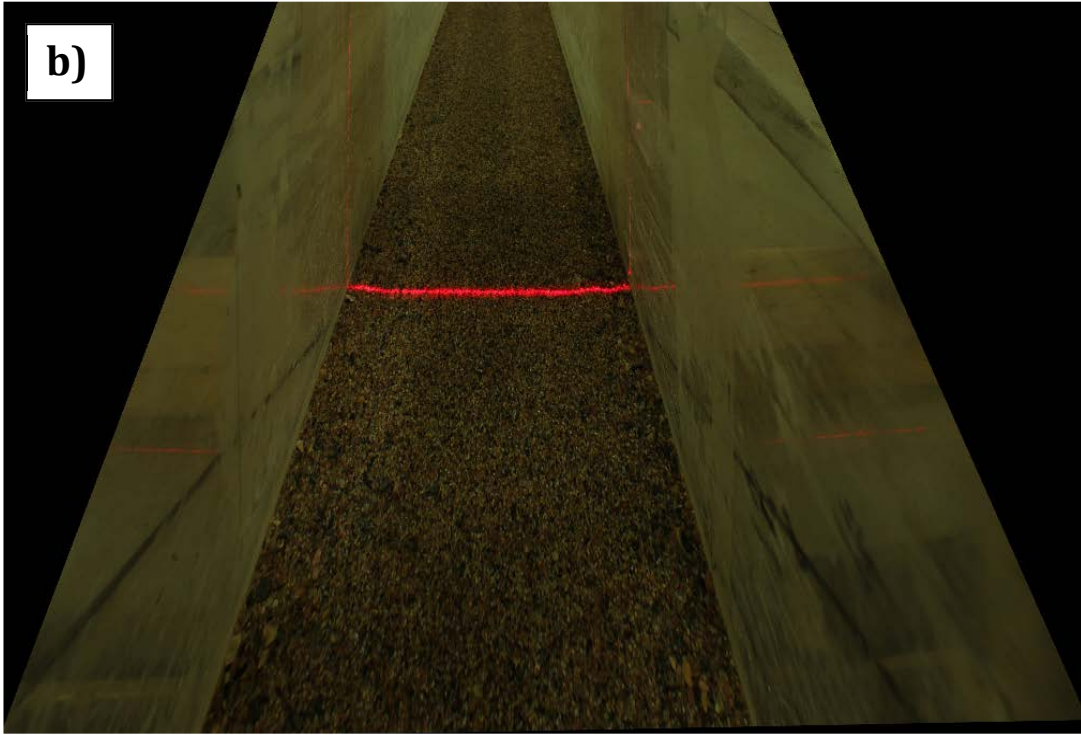


**Figure 13:** Example photo series of the image distortion correction and laser pixel extraction process.

Each cross-section image was composed of pixels, having known elevations. These cross-sections could then be merged together and a kriging routine was used in Surfer 8.0 to generate bed surface digital elevation models (DEMs). The grid was composed of 12,000 cells, 20 cm in the x direction and 10 cm in the y direction. The grid was then bounded by the sinusoidal flume walls to eliminate cells outside of the flume boundary. In addition, a point gauge was periodically mounted on the board system to collect water surface profiles before the flume was drained. Measurements were taken at 26 locations along the flume centerline at 37 cm intervals to capture locations of greatest width (riffles), maximum constriction (pools) and transitional zones. A #200 (0.075 mm opening) sieve was used to periodically capture bedload transport rate at the flumes outlet across different experiments. Bed material samples were collected using a flour paste adhesive sampling technique at seven cross sections in the downstream most section of the flume [Bunte and Abt, 2001]. These sampling sites encompassed two pools, two riffles and three intermediate sections (Figure 14).



**Figure 14:** Sediment surface sampling locations along the flume

The general data collection procedure across all experiments involved: (a) running the flume for a set amount of time with a constant discharge, (b) while running the flume, capture bedload transport at the downstream end with a sieve at 15 minute intervals, (c) collecting water surface measurements with a point gauge just before the flume is shut off, (d) terminating the flow and allowing the bed to drain, (e) gathering bed material samples

in the two downstream most pools and riffle (f) collecting a set of laser images at 20 mm intervals along the flume and process them to develop a bed DEM.

### ***Initial Conditions***

A layer of the concrete sand bed material was graded to a 0.007 slope with a thickness of approximately 10 cm at the entrance to the sinusoidal walls and 5 cm at the downstream end. The 1.58 m inlet was graded flat with immobile cobble sized rocks placed at the upstream most 0.25 meters to prevent inlet scour from occurring. The overall experiment consisted of a set of five runs, designed to simulate equilibrium conditions, dam installation, and dam removal. The set up and execution of these runs is described below.

### ***Run 1: Equilibrium Conditions***

To establish riffle-pool morphology in variable width conditions, the flume had to be supplied with sediment at an equilibrium rate. Several bedload transport equations along with numerical simulation results were used to estimate the sediment feed rate. The Wong and Parker (2006), Engelund and Fredsøe (1976), and Fernandez Luque and van Beek (1976) bedload relations were used to predict equilibrium transport rates based on the flume geometry, discharge, and median grain size of the bulk sediment mixture. As is common across most empirically based sediment transport relationship, bedload transport values varied within an order of magnitude. Wong and Parker produced the lowest transport rate (Table 2), while Engelund and Fredsøe calculated the highest value. Nays2D simulation results produced reasonable median and average feed rates at equilibrium conditions that aligned with the empirical calculations on the same order of magnitude.

The median value was defined as the intermediate value for a central riffle cross section as opposed to the average which was a Nays output for the entire flume. Based on these results, it was decided that 150 grams/minute was a reasonable initial value and the flume would adjust its slope to any initial variability between sediment supply and transport capacity as proposed in Lane's Balance.

**Table 2:** Summary of Calculated and Modeled Equilibrium Feed Rate

Wong and Parker (grams/min)	75.1
Fernandez Luque and van Beek (grams/min)	106.6
Nays2D Median Results (grams/min)	168.5
Engelund and Fredsøe (grams/min)	250.6
Nays2D Average Results (grams/min)	257.5

Additional concrete sand was weighed and separated into bags so that each contained 150 grams of material. The flow valve to the flume was turned on and the discharge was adjusted to maintain approximately 1.5 cm of flow depth at the outlet. This corresponded to a measured average discharge of 0.032 cfs (0.91 l/s). The flume was run for a total of 13 hours while feeding a bag of sediment at the upstream inlet every minute. Periodic bedload measurements were taken over the last 5.38 hours of the run by capturing bedload at the outlet for 60 seconds and weighing it. Approximately 30 minutes before the flow was turned off, a series of water surface elevation measurements were taken in the wide, narrow and intermediate sections along the flume that could be matched to the final bed topography. The discharge was shut off after a total run time of 13 hours as the system appeared to have adjusted to an equilibrium condition. Once the flume was completely drained the laser image system captured a set of laser photographs that would

develop a DEM representing the initial riffle-pool morphology for the proceeding experiments.

### ***Run 2: Dam Installation***

To simulate the installation of a dam (Run 2), the flume was no longer supplied any sediment at the upstream inlet but the discharge remained constant at the flow rate prescribed previously. This condition was run until the system had obtained a new equilibrium slope and minimal sediment transport occurred at the downstream outlet. The discharge was turned off and topographic data collection occurred after 1.33 hours, 2.48 hours, 4.73 hours, 6.85 hours, 11.00 hours, 15.20 hours and 23.58 hours of simulation time. Bedload was captured at the outlet every 15 minutes early in the simulation and every 30 minutes later on. Photographs were also taken in representative central riffles and pools to characterize the grain distribution and to look for any patterns of bed sorting.

After 15.20 hours, bedload transport had decreased significantly and the system seemed to be approaching a stable slope. Once a data set was collected, the flume was run for another 8 hours to confirm this. At 23.58 hours, bed material samples and a final topographic photo set was taken.

### ***Run 3: Dam Removal: Constant Sediment Feed Rate***

To create a dam removal scenario, sediment had to be reintroduced to the starved bed in a controlled and realistic manner. To do this, the initial feed rate of 150 grams/sec was supplied to the well-armored bed and fed at a constant rate every minute. The flume was once again periodically stopped in one-hour intervals with bed topography data collected at 1.17 hours, 2.35 hours, 3.47 hours and 4.5 hours. The sediment transport rate

measured at the outlet was approximately equal to the supplied feed rate by the end of this experimental run.

#### ***Run 4: Dam Installation #2***

Before proceeding with another dam removal scenario, the flume had to revert to an armored, low transport capacity state. The flume was run overnight for a total of 28.62 hours, with data collected to serve as baseline topography for the proceeding experiment. Run 4 was stopped when sediment transport at the flume outlet declined to about 2.2 g/min. The flume at the end of Run 4 was considered well armored and used as an initial condition for the next variable sediment supply experiment.

#### ***Run 5: Dam Removal #2: Sediment Pulse***

Run 5 differed from the prior feed increase experiment (Run 3) by incorporating the pulsative nature of sediment releases and the sorting of evacuated reservoir deposits by grain size class during a dam removal. The sediment pulse was sized to the volume of sediment needed to completely fill in the pools present at the end of Run 4 and cover the resulting plane bed with a carpet of sediment with a thickness of one  $D_{50}$  of the pulse material, similar to other sediment pulse experiments (e.g., Sklar et al., 2009). The total mass needed to fill in the topography was calculated to be 15.69 kg and would be distributed at a rate of 600 grams/minute over 26.16 minutes. This meant the pulse would be fed at a rate 4 times greater than the original equilibrium feed rate, as used in gravel augmentation pulse experiments [Sklar et al., 2009]. To account for reservoir sediment stratification, the introduced pulse was to be well sorted, with the grain size class falling closely in line with the  $D_{50}$  of the original distribution, ranging from 0.83 – 1 mm. This was

done with a sieve shaker and a range of 7 sieve sizes to evenly distribute the material and allow passage through the appropriate screen. Only the sand that had passed the 1mm sieve and retained on the 0.83 mm was kept for the experiment.

Using the constant discharge consistent throughout all experiments, the flume was run with sediment pulses introduced. Bags containing 600 grams of the well sorted sediment were fed at the upstream inlet every minute for the duration of the calculated fill volume. Visual observations of the location of the sediment pulse front were recorded every minute until it reached the flume outlet. At this point bedload measurements were taken every 5 minutes to monitor the pulse response. The flume was drained and restarted periodically throughout the experiment to collect topographic scans of the bed. Topographic scans were collected initially at 5 minute intervals to capture any initial rapid changes, and the frequency of scans was reduced to 10 minutes, 20 minutes and finally multiple hours as equilibrium conditions were approached. The experiment was run until the entire pulse of sediment was evacuated from the system, which occurred after 711 minutes of run time.

## RESULTS

### Elwha Observations and Analysis

#### *Sequential Pool Filling and Evacuation on the Elwha*

The baseline dataset from July 20, 2011 from before dam removal shows three clearly defined riffle-pool sequences within this reach as depicted with the brown line in Figure 15 and a typical riffle-pool backwater profile that occurred with 2,340 cfs of discharge during the time of the survey with an average bed slope across the reach of 0.0063 ft/ft.

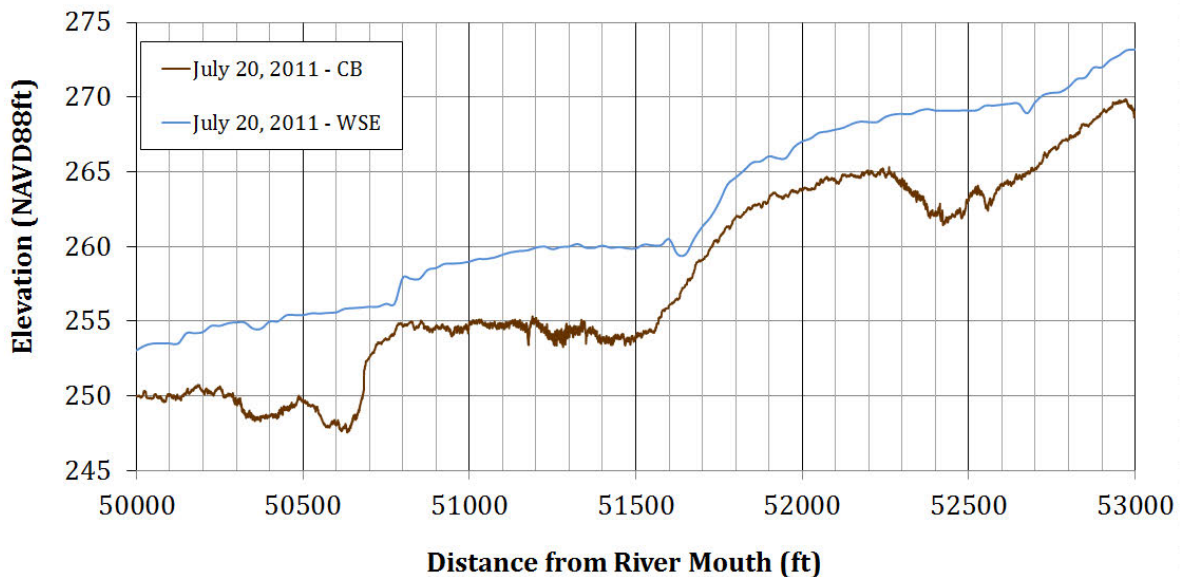


**Figure 15:** July 2011 channel bed and water surface profiles of the study reach before dam removal.

Advancing forward to the May 9, 2013 data set, locations of former pools have aggraded significantly, and the morphology has approached a plane bed condition with an identical average slope of 0.0063 ft/ft (Figure 16). At this point in time Glines Canyon Dam had

been partially removed and fine reservoir sediment was readily available to be transported. The water surface profile that developed is that of a flatter, shallower system under quasi-normal flow condition. This reduction of backwater effects induced by reduced riffle relief suggests an increase in sediment transport capacity.

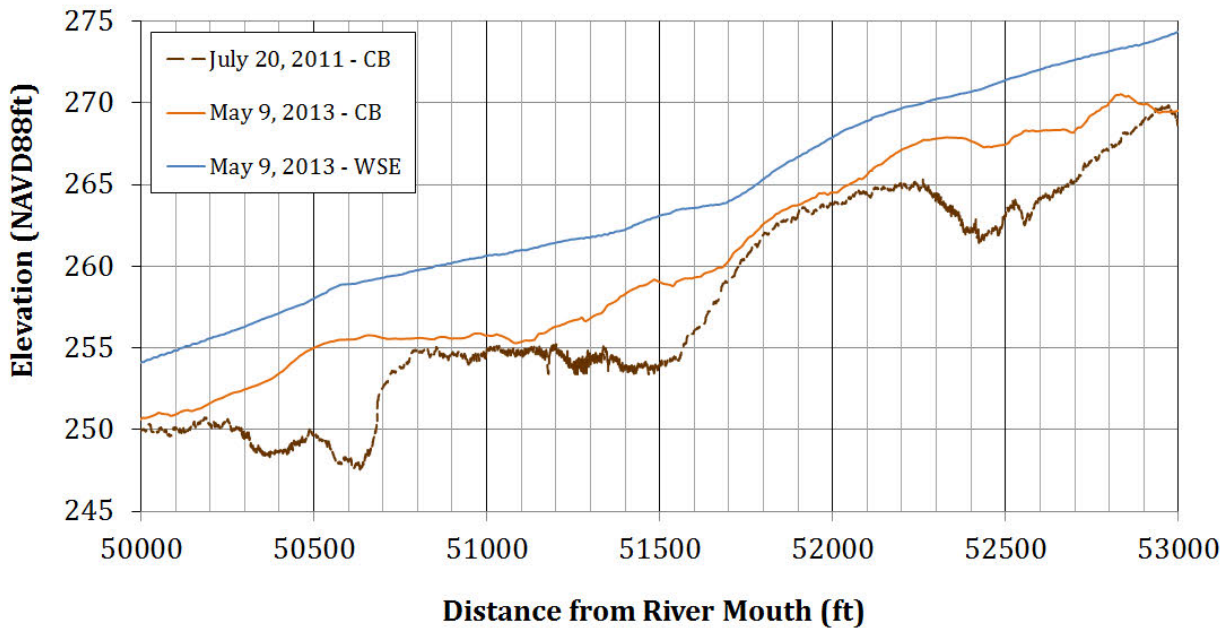


**Figure 16:** May 2013 channel bed and water surface profiles of the study reach during dam removal depicting temporary pool filling.

In contrast, the August 1, 2013 profile shows the reemergence of pools in their former locations suggesting an external control on where pools will form in this reach (Figure 17). In addition, low flow conditions emphasize the backwater effects that have reemerged due to the redeveloped bed morphology with an average slope of 0.0064 ft/ft. This morphodynamic adjustment suggests that the fine sediment that had filled the pools previously was evacuated coupled with a sharp reduction in upstream supply.

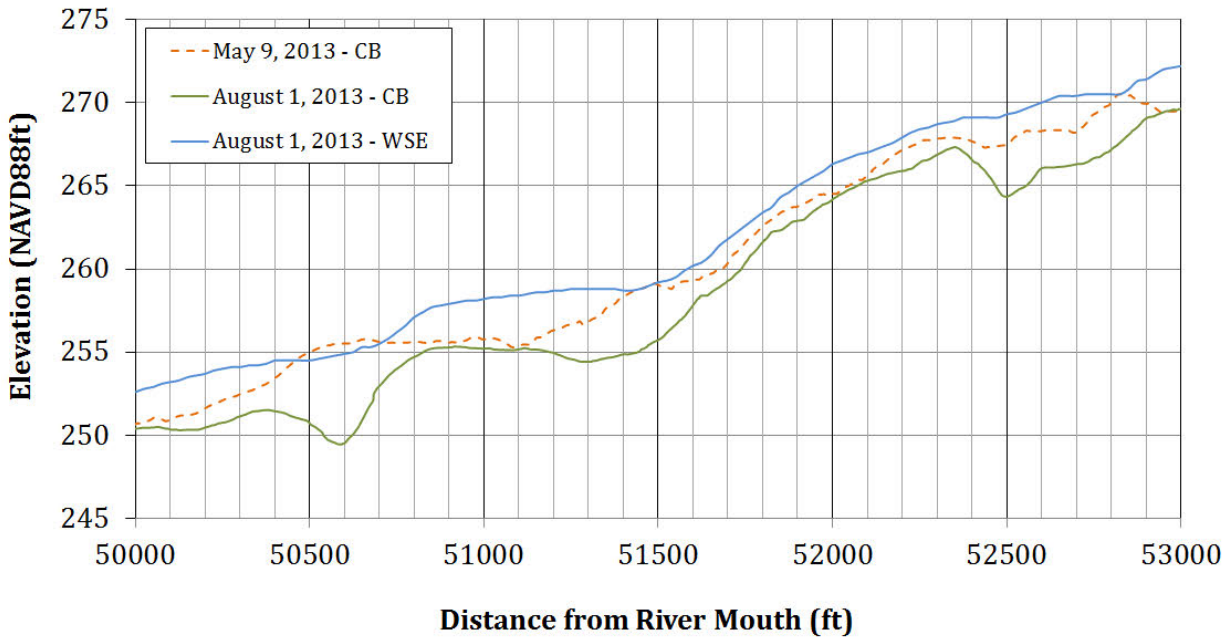


**Figure 17:** August 2013 channel bed and water surface profiles of the study reach showing pool evacuation

### ***Hydrologic Regime During Dam Removal***

Analyzing stream flow data over the duration of the dam removal project to date (September 10, 2011 to June 26, 2014) shows a dual hydrologic regime driven by both rain and snowmelt, typical of Pacific Northwestern watersheds at moderate elevations [Climate Impacts Group, 2014]. In a typical water year there is a peak due to winter storms, a recession and then another peak in late spring or early summer due to snowmelt runoff and “rain on snow events”. In addition, the overall magnitude of peak flows showed the lack of a major channel forming flow event exceeding bankfull conditions (Figure 18). Bankfull stage is typically defined as the discharge that fills the main channel and begins to spill onto the floodplane [Leopold, 1994]. It is considered very influential on geomorphic processes and often characterized as the discharge that has a recurrence interval of 1.5-2 years [Leopold, 1968; Williams, 1978; Andrews, 1980]. After calculating the return periods

of various flow events based on 86 years of available annual peak discharge records, bankfull conditions could be characterized. The lowest value in the series of 4,680 cfs became the 1-year discharge and linear interpolation determined the 2-year flow to be 13,848 cfs. During the time period of interest only three instantaneous peaks reached the 1.5-year value of 10,300 cfs and no events exceeded the 2-year flow. This period of relatively mild hydrology suggests that there were likely no overbank flows and major channel forming discharges probably did not occur. Therefore, the channel width may have acted as an important driver in the geomorphic processes that did occur such as the observed pool filling and evacuation.

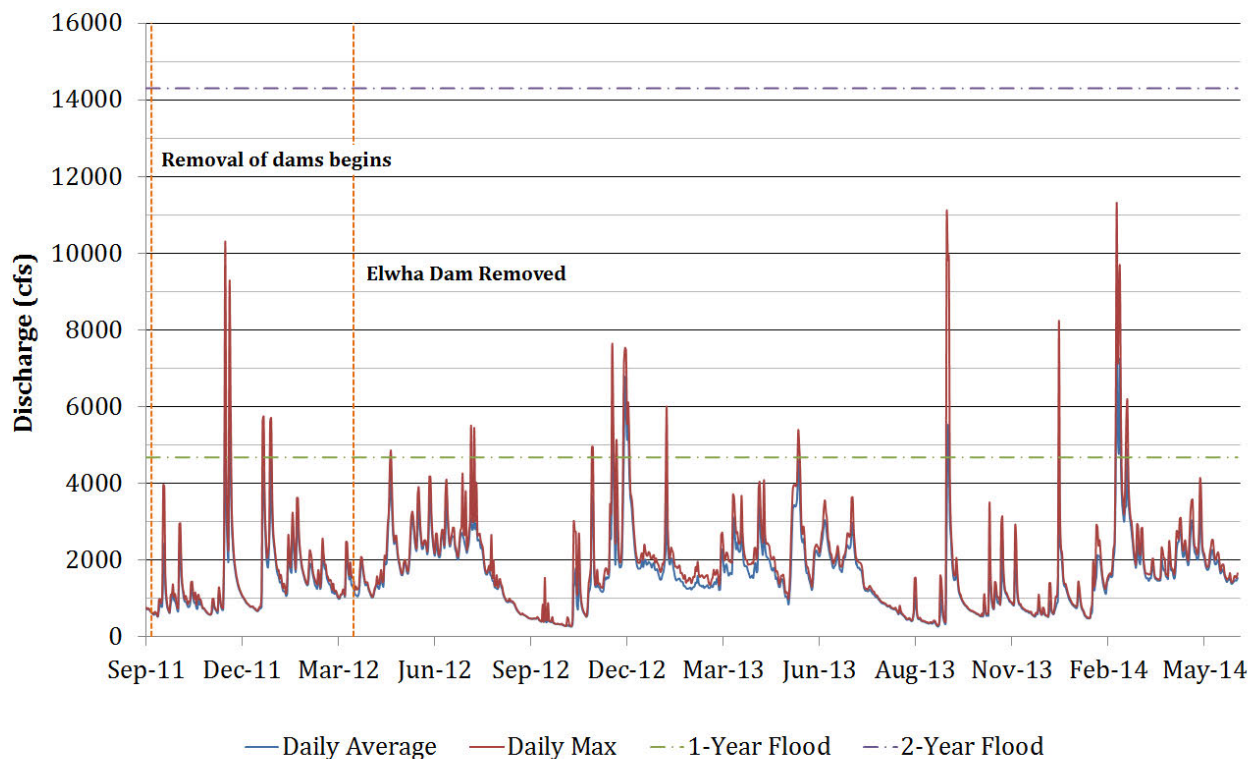


**Figure 18:** Hydrologic Record of the Elwha during the dam removal time period at: USGS 12045500 ELWHA RIVER AT MCDONALD BR NEAR PORT ANGELES, WA

### ***Bed Evolution and Width Observations***

The defined channel width of the study reach identified with Google Earth and spatially aligned with bed topography surveys is presented below. Over the time frame of interest (2009-2013) this reach showed slight lateral migration around meander bends and maintained a relatively constant bankfull width throughout, with an average of approximately 180 ft. (Figure 19). The bathymetric survey data shows the three pools coinciding with the most constricted channel width and riffles forming in the widest locations (Figure 19). These trends in variable bankfull channel width coinciding with the locations of riffles and pools align with observations made by Richards (1979). As described previously, after a temporary disappearance in the May 9, 2013 survey, pools reemerge in the August 1, 2013 survey, which suggests that these locations of minimum channel width provide an important local control on pool persistence over a short time frame under conditions of dynamically changing sediment supply.

In Figure 20, the water surface profiles from all three bathymetric surveys are presented. With the riffle-pool morphology present, the water surface displays backwater effects due to significant topographic relief. However, in the May 9, 2013 survey with subdued riffle-pool topography, the water surface is much flatter and has reduced backwater effects. On August 1, 2013, the riffle-pool morphology returned along with the redevelopment of backwater effects.

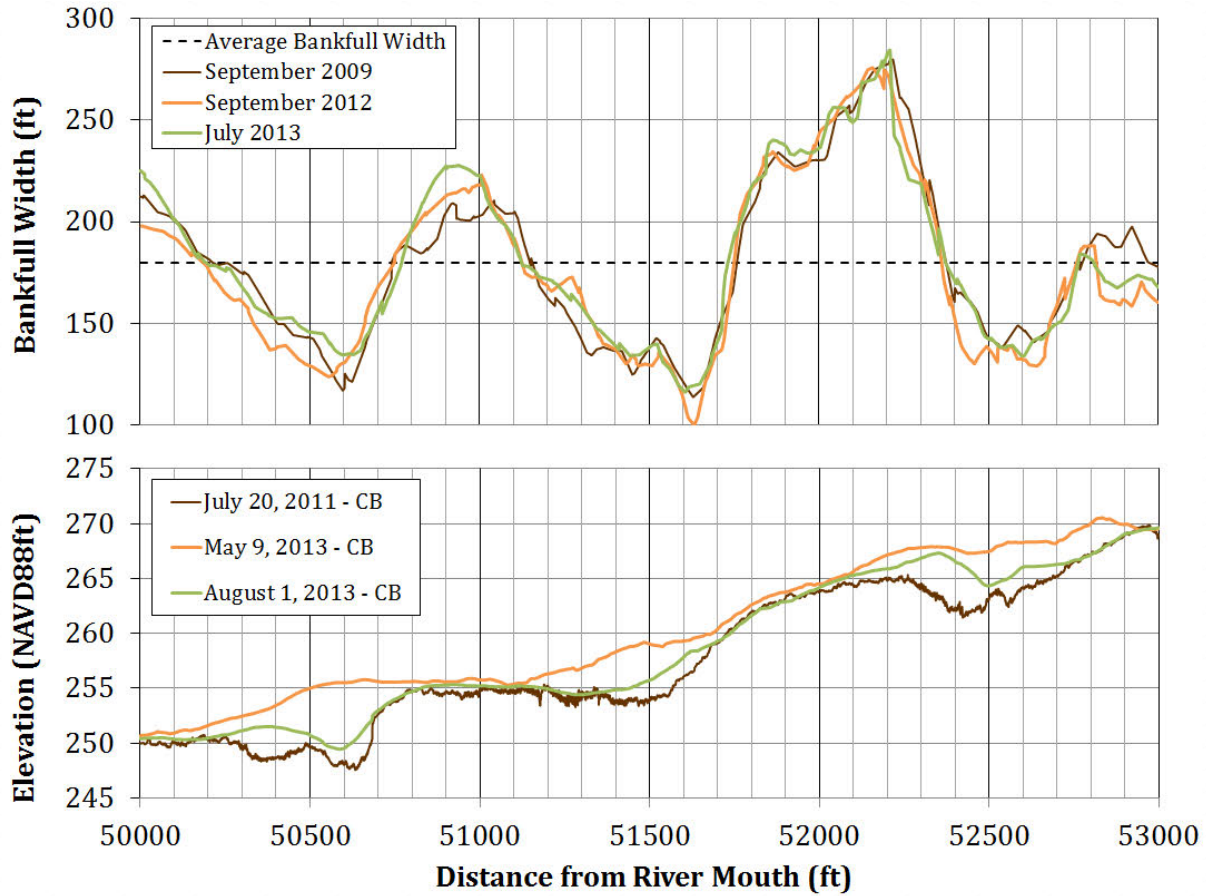


**Figure 19:** Coupling of bankfull channel width from Google Earth and bathymetry from in the Elwha Study Reach.

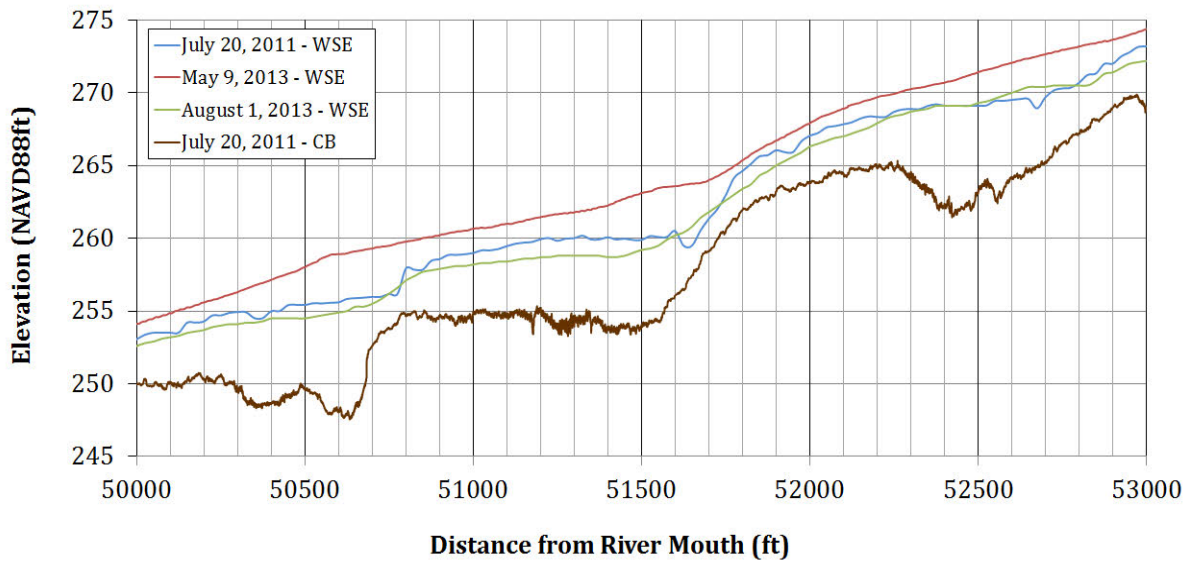


**Figure 20:** Time series of water surface profiles showing the disappearance and reemergence of a backwater profile in the Elwha study reach.

## Experimental Results

### *Bedload Transport Results*

Measurements of the bedload transport rate were taken during all five experimental runs to quantify sediment transport and identify any trends towards dynamic equilibrium based on the initial conditions of that particular run (Figure 21). During Run 1, the flume adjusted to a constant supply of 150 grams/min in approximately 12.5 hours, equilibrating transport at the outlet with the provided supply. This justified starting the second run in which no supply was provided and in approximately 25 hours it reached a no supply condition and the first dam removal experiment could begin. During Run 3, supply was returned the original rate of 150 grams/min and the flume responded quickly by returning its transport capacity to the supply rate in 4 hours time.

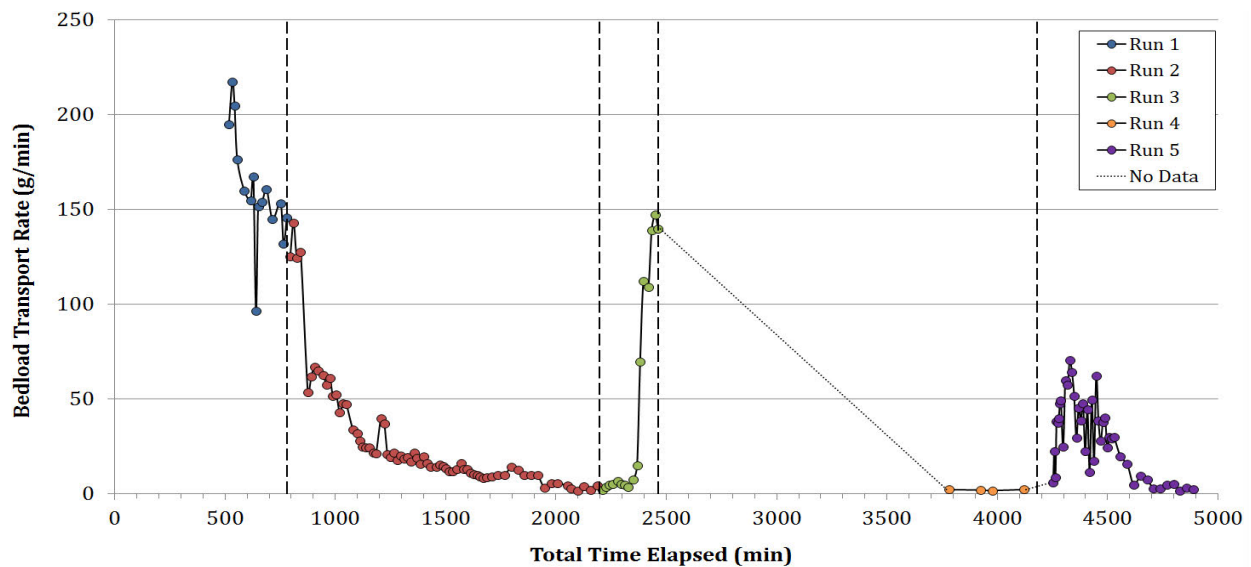


**Figure 21:** Bedload transport rates at the flume outlet across all five experimental runs. Vertical lines indicate the start/end of Runs 1-5.

Before the second pulse experiment, the flume was run for 24 hours with no supply and returned to a starved condition. Finally, a sediment pulse was introduced over 27 minutes and the flume responded by distributing the majority of the pulse over a 6-hour period with the peak feed rate being 70.4 g/min at 2 hours and 36 minutes of elapsed time.

### ***Topography and Grain Distributions***

Over the duration of the first run, water surface and bed profiles were taken with a point gage three times (Appendix B). After 13 hours, riffle pool morphology was clearly established and Figure 22 shows the measured water surface and bed profile immediately before the flume was stopped for the final time. The bed profile measurements are also compared with the profile developed using the laser photo imagery system. As expected, pools developed in the most constricted sections of the flume and there is approximately 8 mm of topographic relief across the riffle-pool sequences.

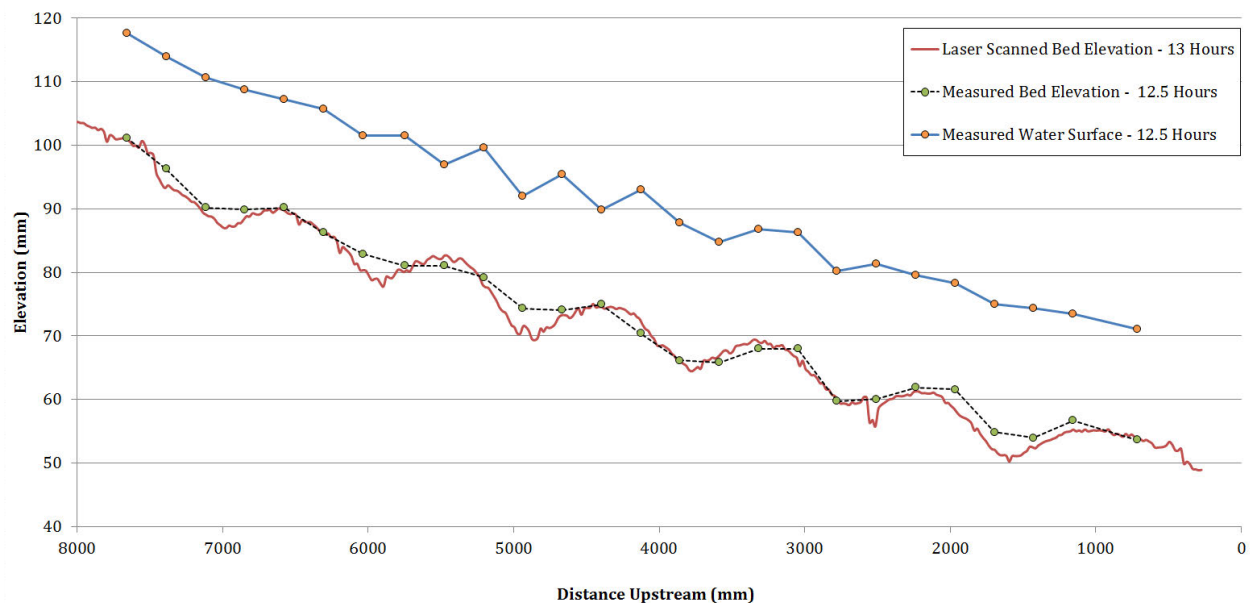


**Figure 22:** Measured water surface and bed elevations of baseline riffle-pool morphology.

A digital elevation model of the final bed topography after Run 1 shows longitudinal and lateral consistency across all six riffle-pool sequences with an average bed slope of 0.0067 (Figure 23). Side bars do develop near the walls of the riffle sections but they do not appear to alter the flow field or sediment transport processes significantly.

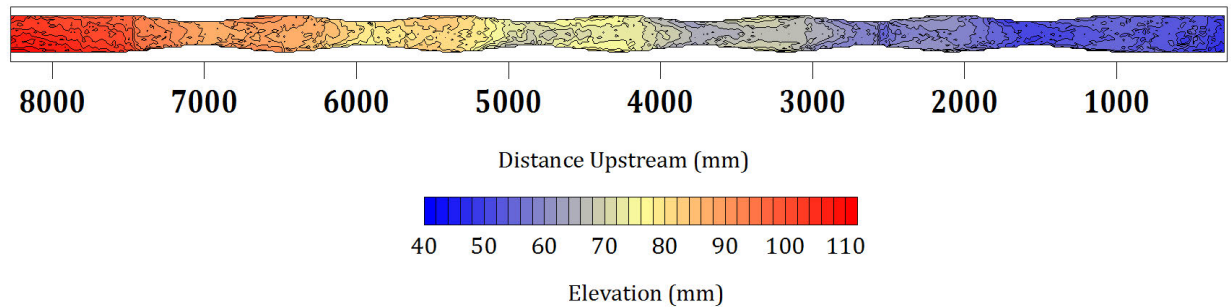


**Figure 23:** Digital Elevation Model of flume bed topography at baseline riffle-pool conditions (Run 1).

Taking this digital elevation model and differentiating each cross section from the mean bed slope distinguished the pools, riffles, and bars that were established (Figure 24). Dark blue sections show pool relief of between 8-10 mm that has developed in the locations of greatest lateral constriction. The intermediate riffles show the aforementioned side bars of approximately 2-4 mm aggradation relative to the central portion of the riffle.

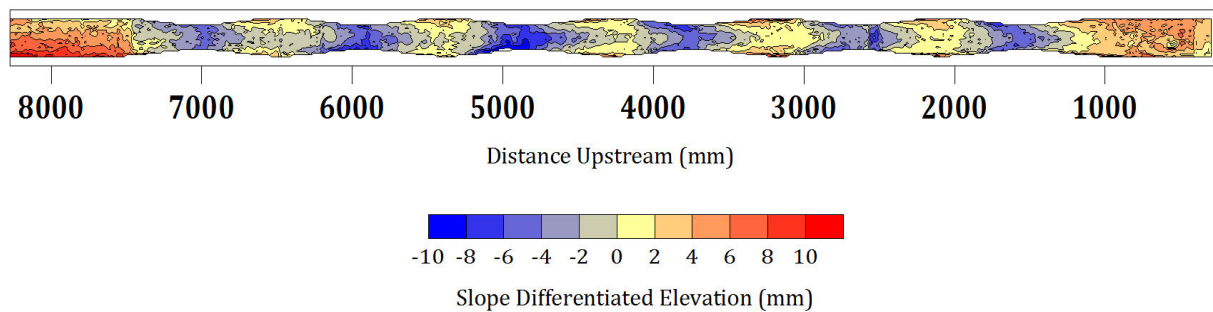


**Figure 24:** Average slope differentiated flume bed topography at baseline conditions showing established riffle-pool morphology (Run 1).

During Run 2, the flume was starved of any sediment supply and the system responded by decreasing its bed slope and armoring its bed. Surface samples of two riffles, pools and transition locations showed overall coarsening of the bed material relative to the original distribution (Figure 25). It should be noted that the distribution after Run 1 had slightly coarsened relative to the original distribution, but the bed surface was not sampled at that time. As expected, the riffles with a  $D_{50}$  of 1.55 mm are slightly coarser than the pools, having a  $D_{50}$  of 1.38 mm.

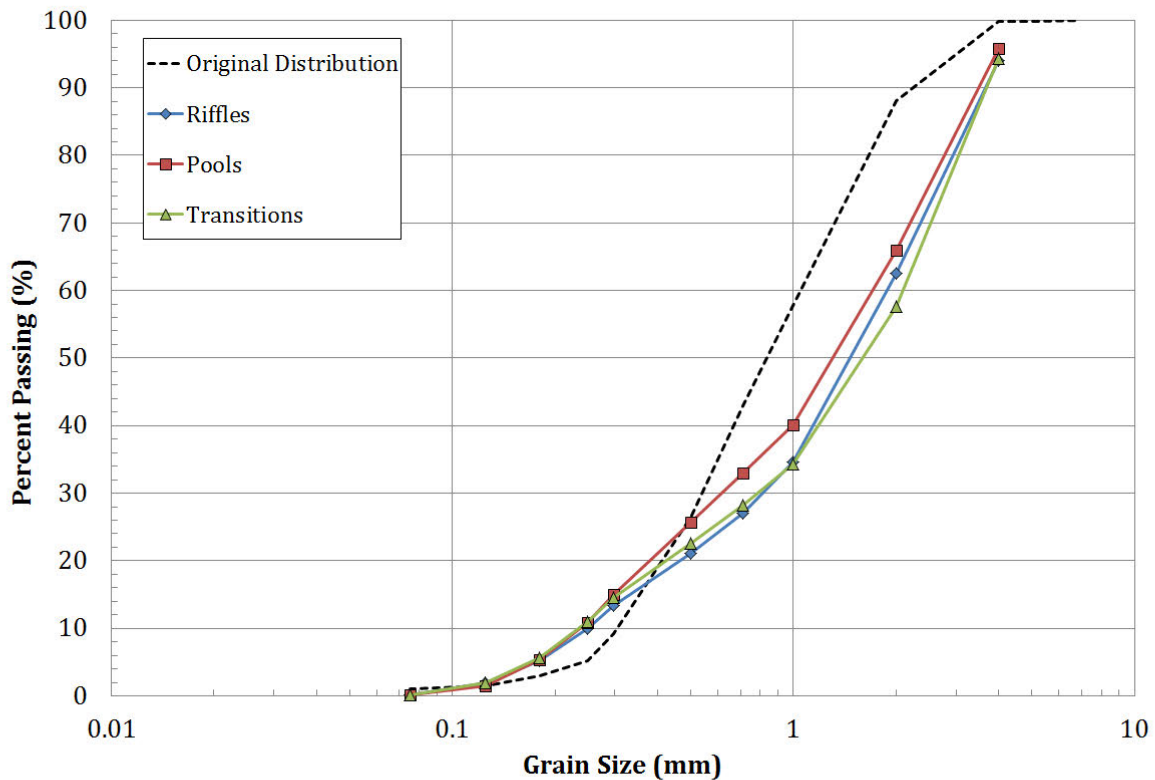


**Figure 25:** Grain size distributions of surface sampled riffles, pools and transitional reaches compared to the original grain distribution showing overall bed armoring (Run 2).

Repeat laser scans of the bed showed a uniform, base level drop and a relaxation of the bed slope to an average value of 0.0037 (Figure 26). Topographic change between the final two scans was negligible, which was justification for concluding Run 2 and moving to the next phase.

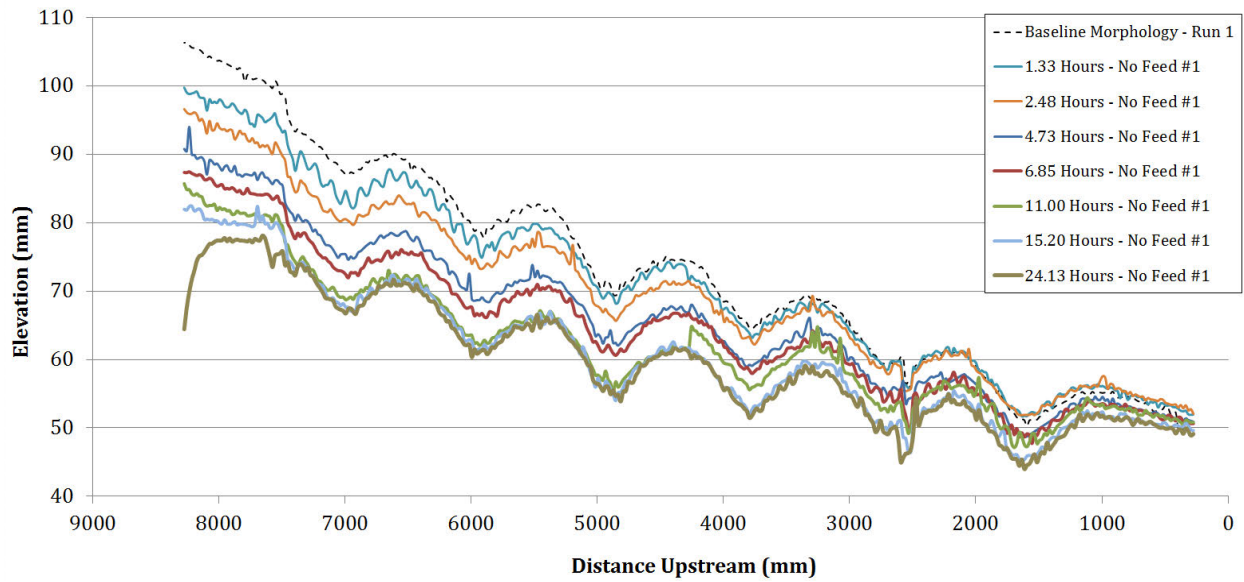


**Figure 26:** Time series of long profiles showing a base level drop and slope decrease over 24 hours of no sediment supply (Run 2).

Similar to Run 1, multiple water surface measurements were taken throughout the experiment and can be viewed in Appendix B. The final measurements show a more relaxed bed topography and water surface profile (Figure 27) but a similar range of relief referenced to the baseline morphology.

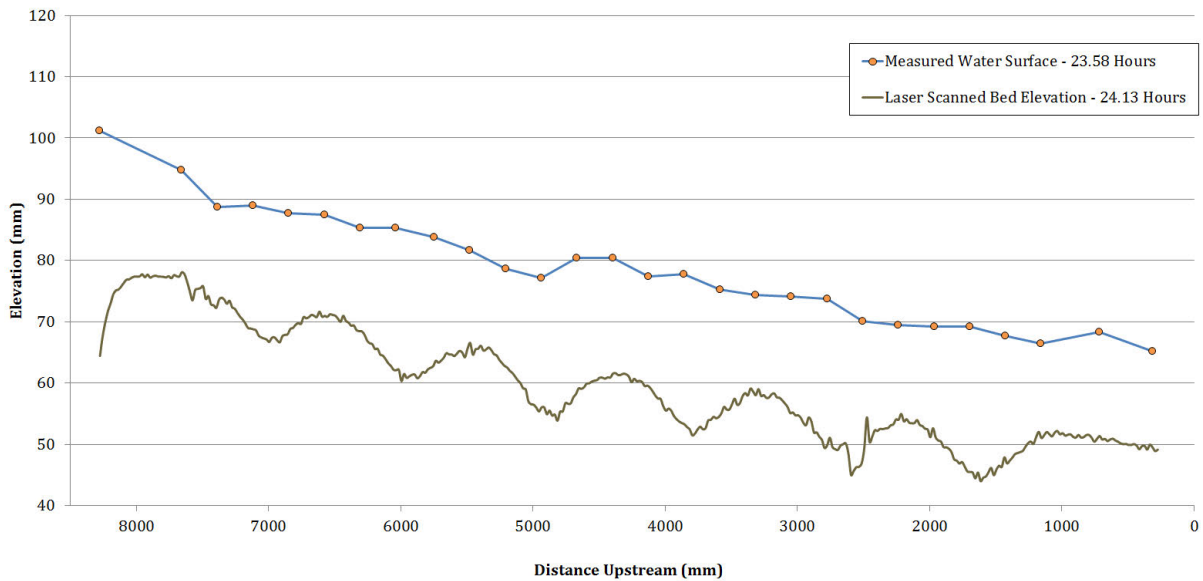


**Figure 27:** Measured water surface and bed elevations of first zero supply condition.

The digital elevation model developed for the end of Run 2 shows relative similarities to Run 1 with the main difference being the total elevation range reduced due to a uniform decrease in the overall bed slope (Figure 28).

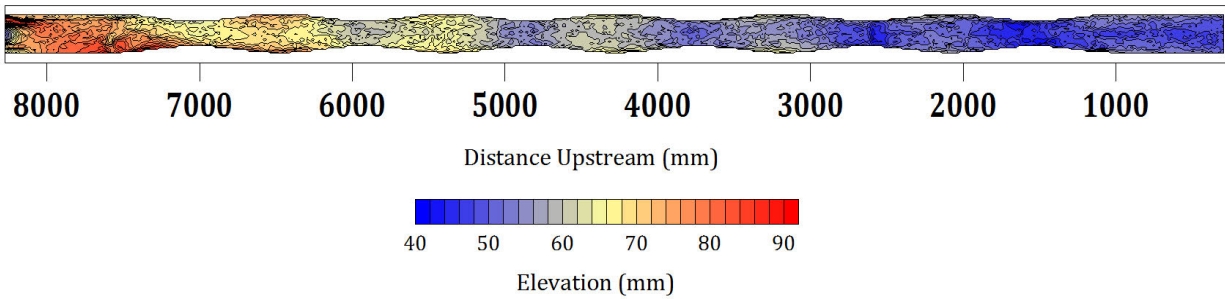


**Figure 28:** Digital Elevation Model of flume bed topography at first zero supply equilibrium condition (Run 2).

The slope differentiated model for Run 2 is very similar to Figure 22 with well-defined riffle-pool sequences, identical relative pool depths and minor side bar formation in the riffle sections (Figure 29).

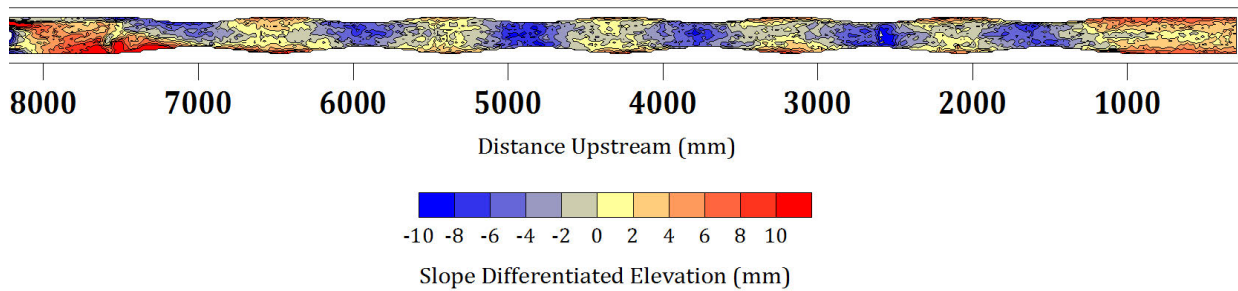


**Figure 29:** Average slope differentiated flume bed topography at zero supply equilibrium condition (Run 2).

The first increase in sediment supply occurred over Run 3 during which the original supply of 150 grams/minute was resupplied to the flume. Repeat topographic scans over 4.5 hours showed uniform aggradation in the riffle-pool sequences of 6-7 mm along the entire flume (Figure 30). Along with net aggradation, a steepening of the bed slope to an average value of 0.0056 occurred.

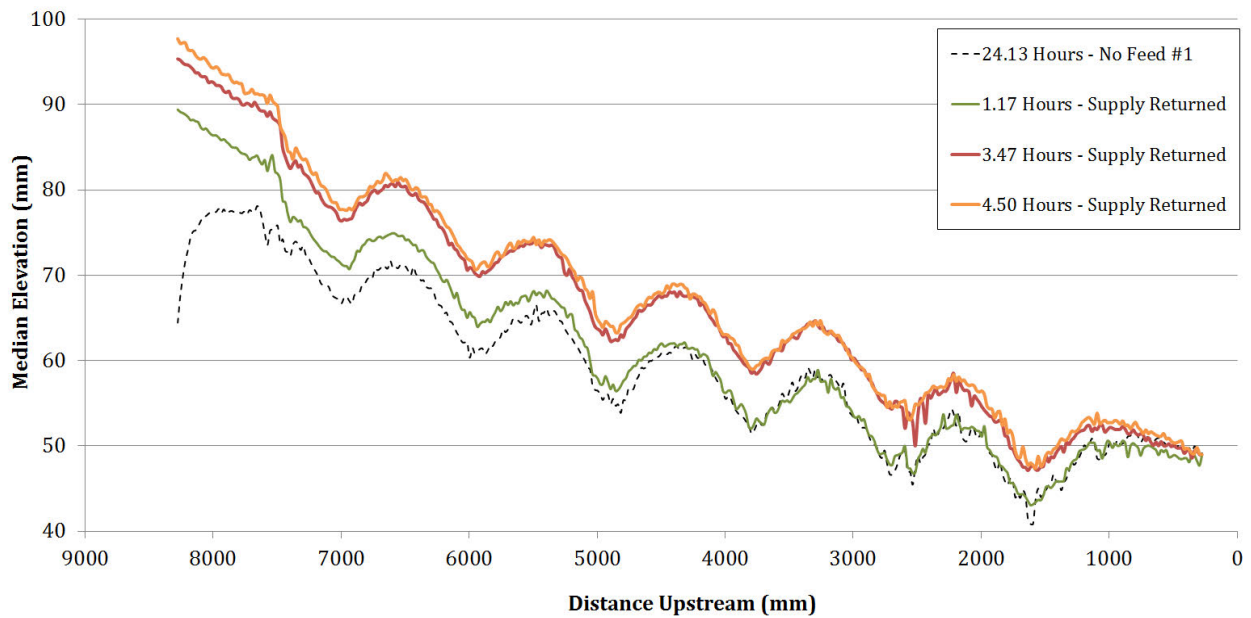


**Figure 30:** Time series of median elevation long profiles showing uniform aggradation across all riffles and pools along with a slope increase after supply was returned (Run 3).

DEMs of topographic scans with the baseline DEM from the end of Run 2 subtracted out show uniform aggradation represented by the orange and red color scheme (Figure 31). Deposition first occurs at the flume inlet where sediment is supplied and migrates downstream until the bed slope had equilibrated to transport the sediment supply.

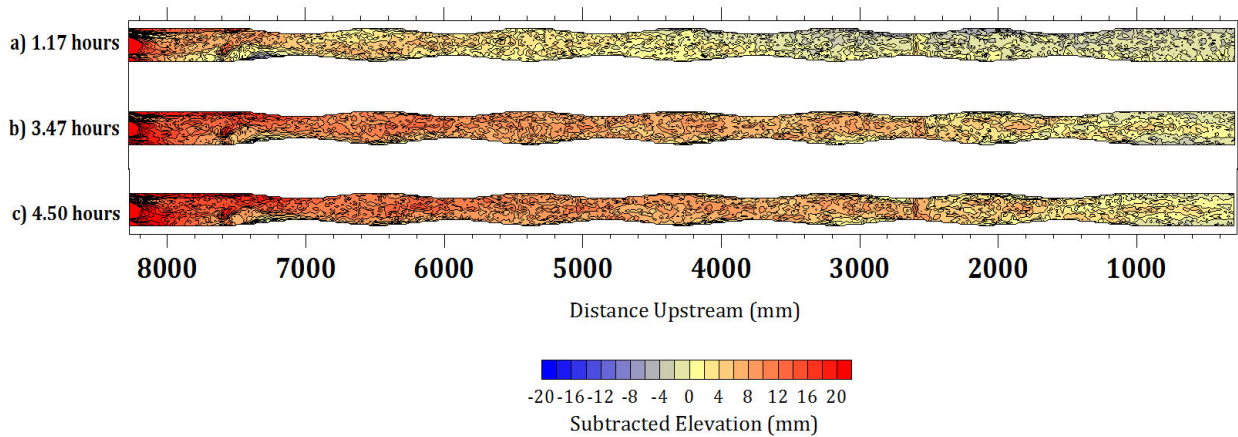


**Figure 31:** Time series of flume bed topography DEM's subtracted from the baseline zero supply elevations at equilibrium after Run 2.

The purpose of Run 4 was to return the bed to an armored state similar to its condition at the end of Run 2, so that an equivalent baseline condition could be provided for another sediment pulse experiment. During Run 4, after 28.62 hours of no supply, sediment transport rates were once again approaching zero (Figure 21). Figure 32 compares the long profiles at the ends of Run 2 and Run 4 and shows that they were very similar.

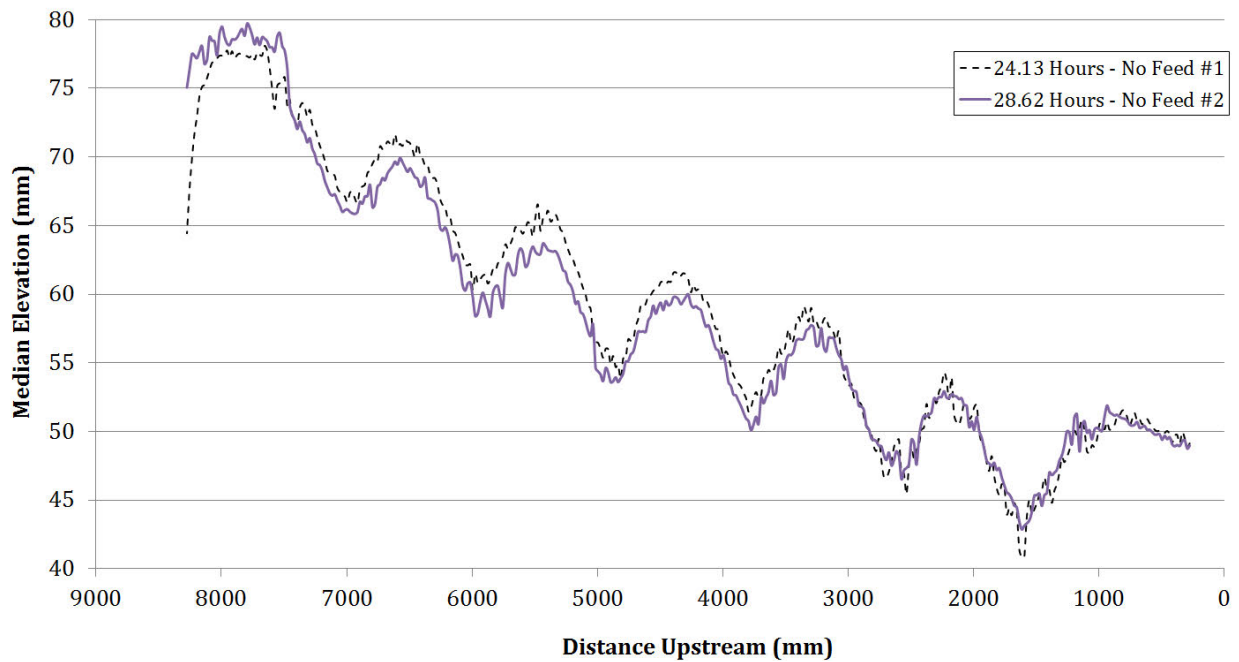


**Figure 32:** Comparison of the no feed long profiles from Runs 2 and 4 to confirm similar baseline conditions preceding dam removal experiments.

A DEM of the bed topography from Run 4 (Figure 34) shows similarities to the relief established at the end of Run 2 (Figure 26). The only noticeable difference is some preferential scour along the right bank of the two upstream most riffle-pool sequences, likely due to entrance effects.

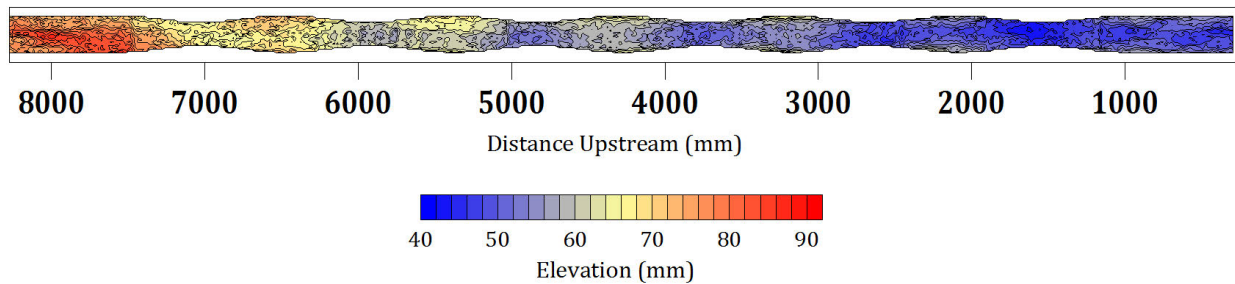


**Figure 33:** Digital Elevation Model of flume bed topography at second zero supply equilibrium condition.

A mean slope differentiated elevation model shows consistent riffle-pool morphology along with small side bars in the riffles as observed in previous runs (Figure 34). In addition, the preferential scour along the right side of the flume is even more evident but appears to subside farther downstream.

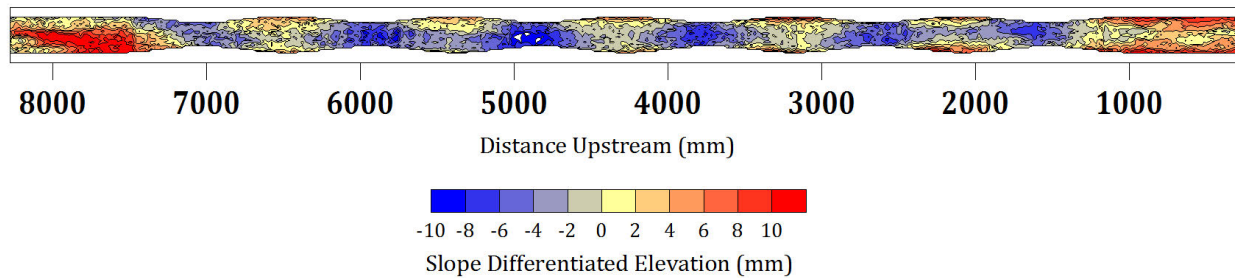


**Figure 34:** Average slope differentiated flume bed topography at second zero supply equilibrium condition

In Run 5, we introduced a pulse of well-sorted sediment having the volume to fill in the pools and minimize riffle-pool relief as observed in the field. Figure 35 shows long profiles of the bed elevation from repeat scans during the first 27 minutes of the experiment when sediment was supplied at 600 grams/min. A dramatic steepening was observed in the two upstream riffle-pool sequences as they responded to this dramatic increase in sediment supply. At 27 minutes the average bed slope reached a maximum value of 0.0067 before it began to relax.

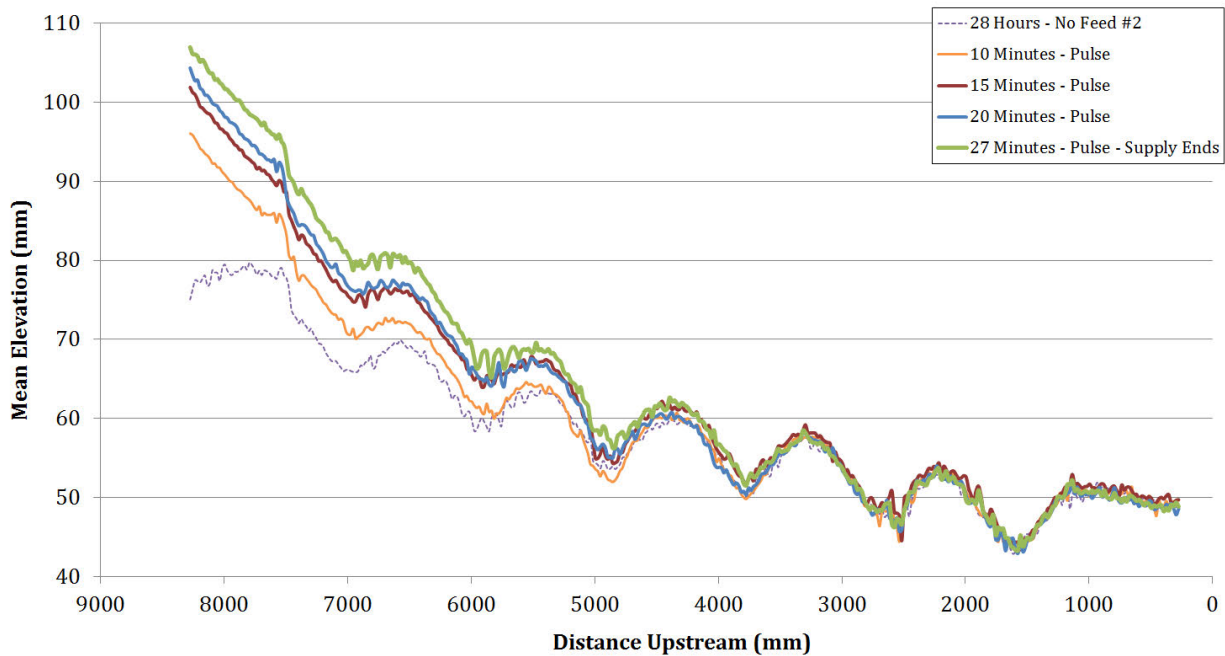


**Figure 35:** Time series of long profiles during introduced sediment pulse showing a dramatic upstream steepening of the bed slope.

Long profiles of the flume bed after the pulse was supplied in its entirety show an immediate reduction in slope as the pulse propagates through (Figure 36). At 47 minutes, the upstream most riffle-pool sequence began to relax and primary aggradation shifted to the second and third riffle-pool sequences. A major period of base level reduction did not begin to occur until after the scan at 106 minutes and the entire system approached its prior state.

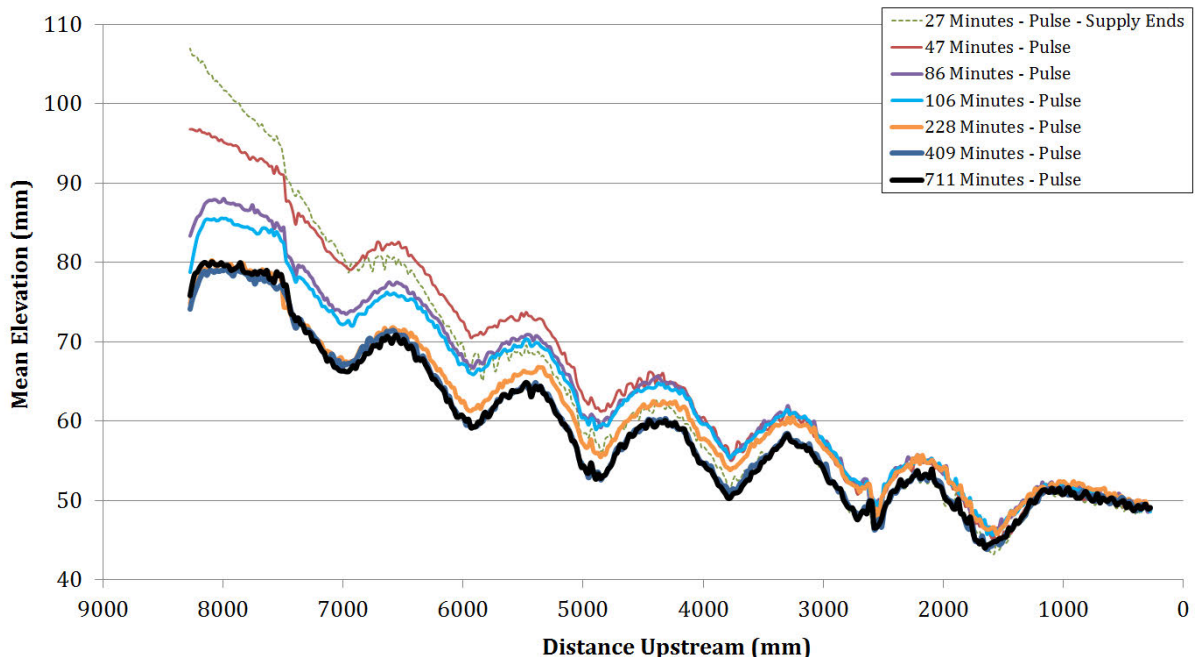


**Figure 36:** Time series of long profiles after sediment pulse has been fully supplied showing a relaxation of the bed slope (Run 5).

A time series of DEMs subtracted from the sediment starved baseline condition (Run 4) show how the pulse propagated through the system (Figure 37). The dashed line indicates where the supplied pulse had reached completion at 27 minutes. Between 47 minutes (Figure 37g) and 66 minutes (Figure 37h), the pulse had reached its dispersive peak as shown by the locations of red coloration located farthest downstream. At that point the system was able to move any pulse sediment through with ease and began to degrade the bed.

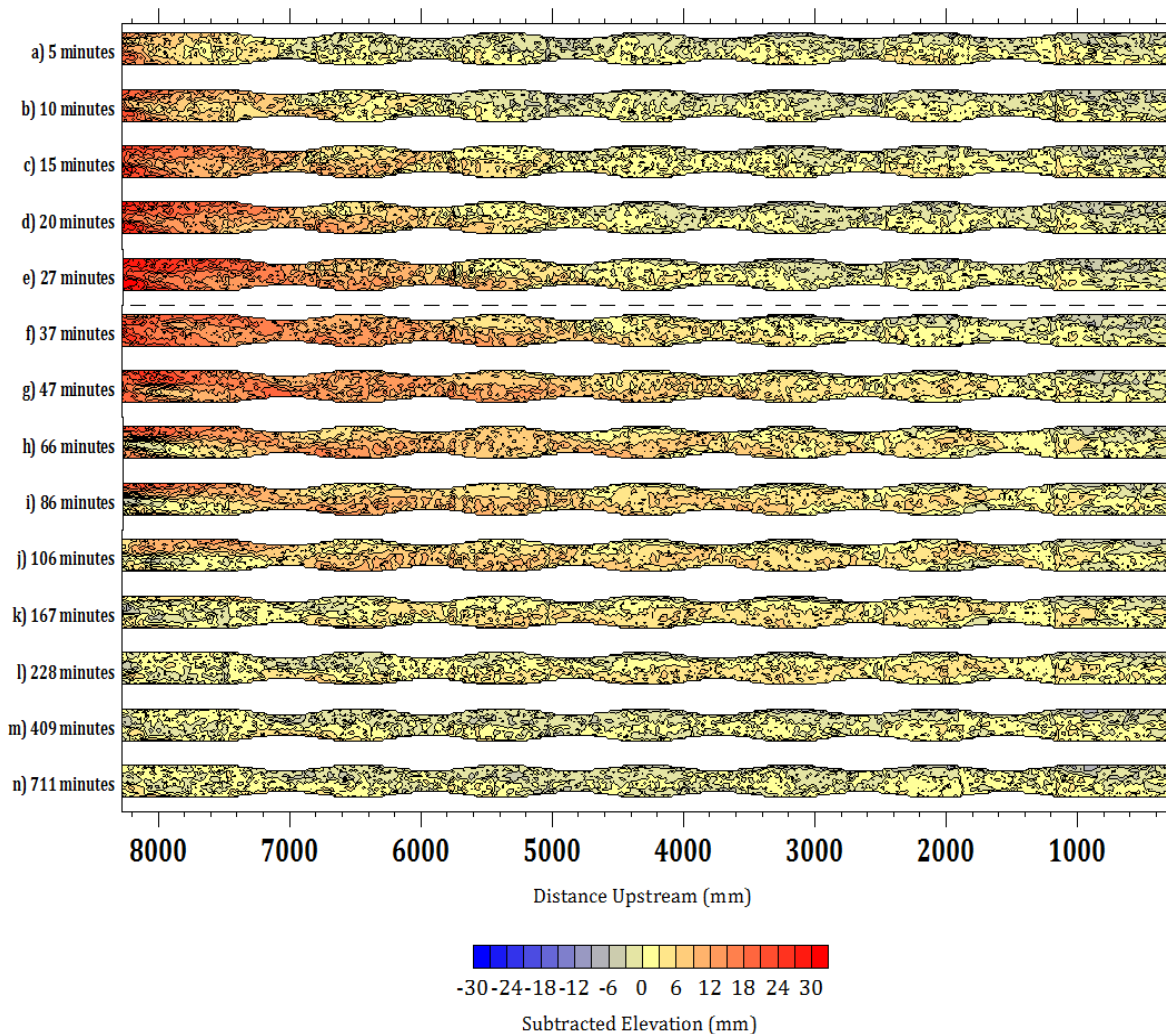


**Figure 37:** Time series of flume bed topography DEM's subtracted from the final topography in Run 4.

### ***Pulse Dynamics***

The front of the pulse introduced in Run 5 was visually tracked as it migrated downstream to the outlet (Figure 38). The black dashed line indicates when the sediment feed was stopped after 27 minutes. Several photos documenting its movement can be seen in Appendix C. The front moved steadily with time and continued to move consistently even after the supply was stopped. After 69 minutes the pulse had reached the outlet and bedload transport measurements began.

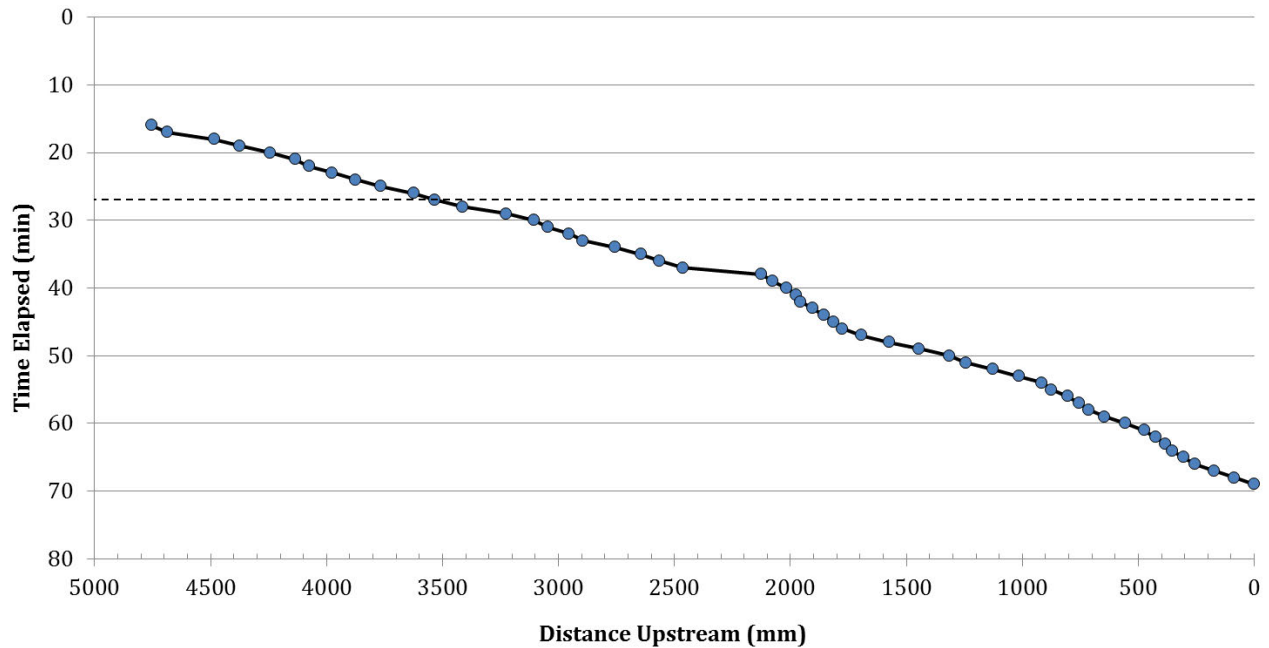


**Figure 38:** Downstream location of the sediment pulse front through time. The dashed line indicates when upstream feed was terminated.

A time series of long profiles differentiated from the baseline elevation was plotted in Figure 39 to offer a comparison with Figure 5C and show how the magnitude of the pulse propagates longitudinally through the flume and eventually relaxes to the baseline condition after nearly 12 hours. A moving average over a 0.48 m window was used to eliminate noise from the differentiated elevation data extracted from long profiles.

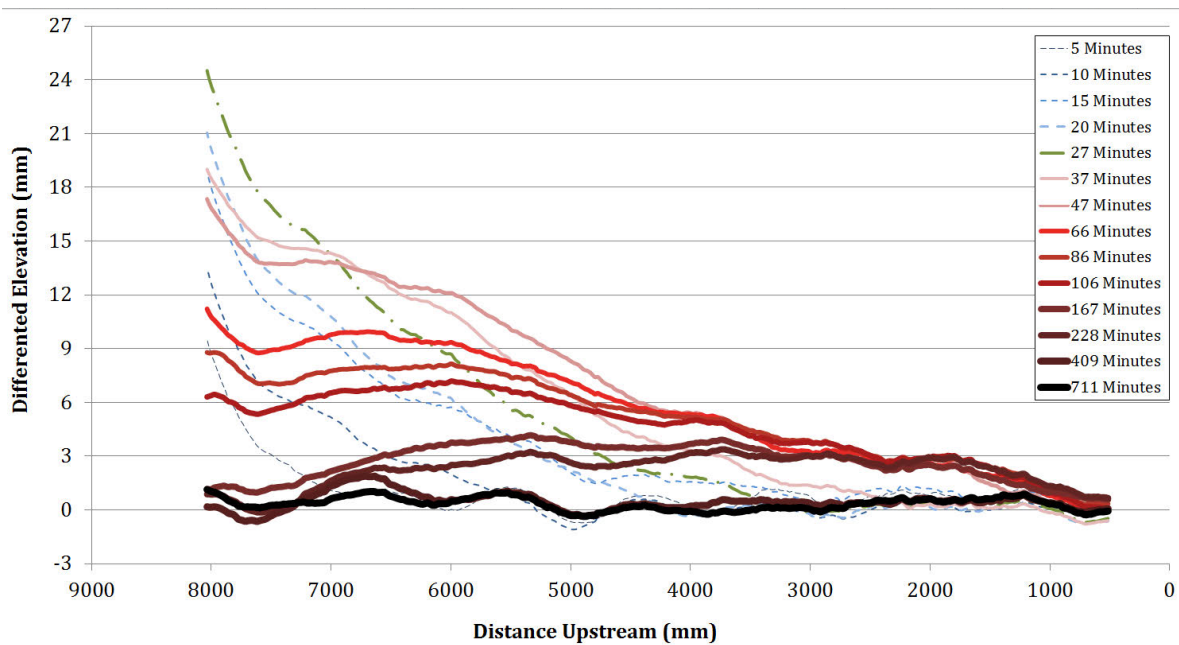


**Figure 39:** Time series of long profiles during the pulse experiment differentiated from the baseline condition in Run 4.

The cumulative sum of the differentiated elevation data is shown in Figure 40. These data indicate that the pulse was dominated by dispersion, rather than translation when compared with Figure 5D. The mode of vertical distribution is clearly defined as the pulse migrated through the flume (Figure 40). At 47 minutes the system hit its cumulative elevation peak and then proceeded to go through net degradation as it was able to begin transporting significant amounts of pulse sediment through.

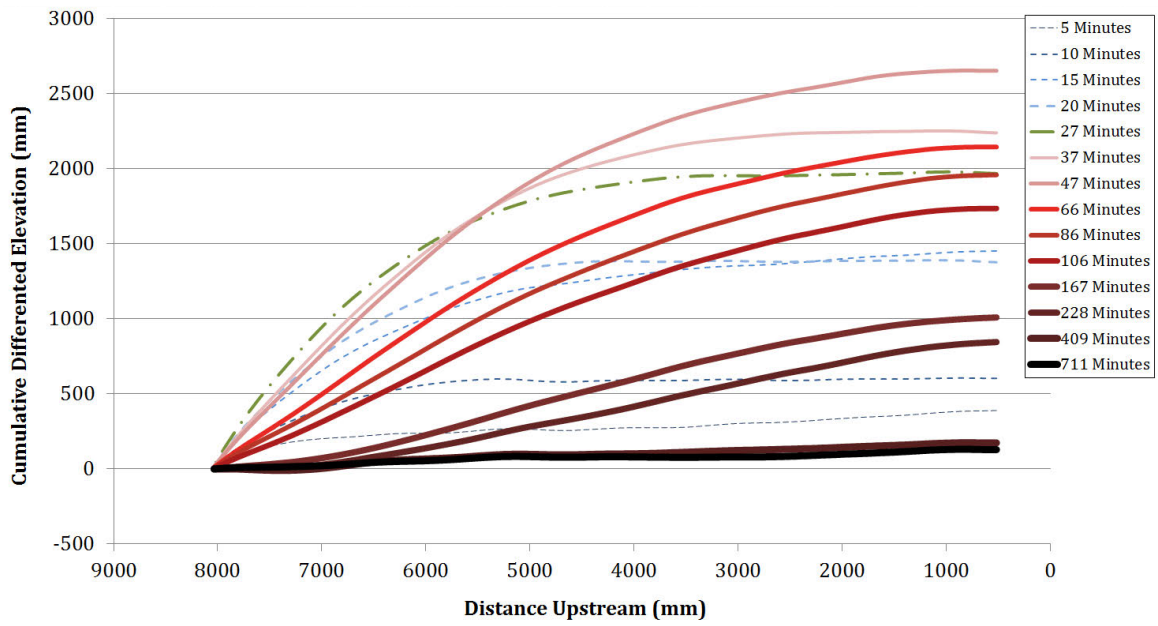


**Figure 40:** Time series of long profiles differentiated cumulatively from the armored condition at the end of Run 4.

## DISCUSSION

### ***Riffle-Pool Morphology and Channel Width***

Channel width has been shown to exert a local control on the development of riffle-pool morphology in certain environments [de Almeida and Rodriguez, 2012] and lead to pool maintenance through flow convergence routing [MacWilliams et al., 2006]. Riffle-pool systems such as the Elwha develop and maintain riffle-pool topography due to this variable width condition. From the perspective of fluid momentum and sediment continuity, these expansions and contractions create variations in shear stress that induce preferential scour in pools and deposition across riffles.

Field results from the Elwha show that bankfull channel width imposed a local control on the locations of riffles pools from 2011-2013, even when the system is undergoing the dramatic change of a large dam removal. The transient pool-filling apparent in the repeat long profiles and the re-emergence of the pools in the same location, combined with the lack of large, channel-forming hydrologic events, suggests that the downstream changes in channel width provided an important control on the location and persistence of riffles and pools. Therefore, a fixed-wall flume study appeared to be an appropriate analogue for modeling conditions on the Elwha within this time frame. To design these flume experiments, channel geometry and its significance on riffle-pool development was first validated using a numerical model.

The Nays2D model is process-based, and the development of pools and riffles coincident with constrictions and expansions in the numerical model shows that mathematically, fluid and sediment continuity require pool-riffle morphology at

equilibrium. Run 1 of the flume experiments confirms this. The flume experiments provide even more evidence of the importance of width variability on bed topography, though, because in Runs 2-5 the sediment supply was varied dramatically, but still the pools and riffles persisted in the same locations. This persistence of pools and riffles during the sediment pulse run (Run 5) further reinforce this idea, because here even with considerable spatial and temporal changes in the local sediment transport rate, the primary channel adjustment was an overall aggradation or degradation to a new local slope, rather than changing the pool-riffle morphology.

### ***Pulse Dynamics***

We can compare the findings from the sediment pulse flume experiments of Lisle et al. (1997), Cui et al., (2003a) and Sklar et al. (2009) with our results to explore the relative effects of riffle-pool topography and width variation on pulse evolution (Tables 3, 4, and 5). The sediment pulse in our experiment propagated through the flume in a more dispersive manner than what was reported in Sklar et al. (2009). The primary difference between our experiment and that of Sklar et al. (2009) is that while both experiments began from a sediment-starved condition and proceeded without a sediment feed, the present experiment was conducted in a variable-width flume that had antecedent riffle-pool morphology while Sklar et al. (2009) used a constant-width flume with plane bed morphology. The increased dispersion in our experiment is likely due to these differences.

In contrast, our pulse did evolve similarly to experiments performed by Lisle et al., (1997) in which a sediment pulse 10x greater than the equilibrium feed rate was introduced into the center of the channel (Table 3). In Lisle et al.'s (1997) experiment, the channel had developed an alternating bar morphology under a constant sediment feed, and

that feed rate continued while the pulse laterally dispersed in both directions. The upstream diffusion in Lisle et al.'s (1997) experiment was a consequence of the sediment feed interacting with backwater effects created by the sediment wave itself. Both the Lisle et al. (1997) experiment and our experiment developed a sediment wedge. However, unlike the Lisle et al. (1997) experiment, our sediment pulse was unable to diffuse in both directions due to the inlet conditions, where the sediment pulse was supplied, and the fact that there was no upstream sediment feed.

Results from Cui et al. (2003a), where a constant sediment feed was supplied during the pulse introduction and evolution, show dispersive characteristics similar to ours. However, their finest pulse in run 4d (Table 3), which used sediment one-third the grain size of the bed surface material, did have some translating properties that were not observed in our flume study. This suggests that there may be a lower threshold in grain size relative to the bed at which a pulse displays translational characteristics. Cui et al. (2003a) also supplied the entire pulse at once while continuing the equilibrium feed, which caused backwater effects that enhanced pulse diffusion. This pulse also caused pre-existing bar topography to disappear as the added sediment filled in the pools. In contrast, the pulse in our experiment was introduced incrementally at a constant rate, which reduced the influence of any backwater effects. Similar to Lisle et al. (1997), the riffle-pool and side bar topography in our experiment remained intact, suggesting that the rate of addition and overall magnitude of pulse material may influence whether pool filling occurs.

In our physical modeling, variability in the flow field such as backwater effects due to downstream variations in bed topography and eddies in local expansions, along with the relief between riffles and pools, likely trapped some of the pulse locally and limited its

overall magnitude as it moved downstream, causing it to evolve in a highly diffusive manner. By comparing our results to these other experiments, it appears that complexity in the bed topography, width variability, and grain size are all important in determining how a pulse of sediment becomes distributed through a channel. If significant variability is induced by channel width or topographic relief on the bed, the system has a tendency to handle the pulse diffusively. This has been shown by the development of alternate bars in Lisle et al. (1997) and Cui et al. (2003a) as well as variable width and riffle-pool morphology in our experiment. Grain size appears to be influential as well shown by the run composed of fine material in Cui et al. (2003a) and the distribution used by Sklar et al. (2009) (Tables 3 and 4). Both reported quicker responses and propagation along with more pronounced translational tendencies. However, pulse magnitude did not appear to be as influential in determining the mode of propagation, as results from Cui et al. (2003a) were all primarily dispersive even with bedload transport rates 40x greater than equilibrium at times.

The presence or absence of upstream sediment feed appears to be an important control on the relative translation and diffusion of sediment pulses. Experiments where an upstream sediment supply was maintained (Lisle et al., 1997; Cui et al., 2003a) found strongly diffusive pulse evolution, which in part may be explained by the pulse addition causing upstream deposition as the feed material encounters the backwater effect of the pulse material. This diffusional mechanism does not occur in experiments without an upstream sediment supply, and indeed, Sklar et al. (2009) found a significant translational component of pulse evolution in their no-feed pulse experiments. That the present study observed the sediment pulse to evolve almost purely diffusively even without an upstream

sediment supply suggests that the width variation and riffle-pool topography is responsible for much of the observed diffusion.

**Table 3:** Comparison of experimental conditions from pulse flume studies with added feed

	Lisle et al. (1997)			Cui et al. (2003a)								
				Run 2			Run 3			Run 4b		
Flume Dimensions (L x W x D)	160 m x 1 m x 2 cm			45 m x 0.5 m x 3.25 cm			45 m x 0.5 m x 3.25 cm			45 m x 0.5 m x 3.25 cm		
Bed Material (D <sub>16</sub> , D <sub>50</sub> , D <sub>84</sub> ) (mm)	0.35	0.57	1.25	0.50	3.73	5.66	0.50	3.73	5.66	0.50	3.73	5.66
Pulse Material (D <sub>16</sub> , D <sub>50</sub> , D <sub>84</sub> ) (mm)	0.30	0.50	1.20	0.50	2.20	4.76	0.52	3.80	5.28	0.50	0.62	1.19
Pulse Mass(kg)	800			210.68			210.68			205.91		
Duration (min)	45			-			-			-		
Pulse Feed Rate (kg/min)	17.78			-			-			-		
Average Pre-Pulse Feed (g/min)	1780			45			45			45		
Pre-Pulse Topography	Alternate Bars			Alternate Bars			Alternate Bars			Alternate Bars		
Mode of Propagation	Dispersion			Dispersion			Dispersion			Translation		

**Table 4:** Experimental conditions from 5 different runs by Sklar et al. (2009)

	<b>Sklar et al. (2009)</b>														
	Run 7			Run 10			Run 23			Run 9			Run 21d		
Flume Dimensions (L x W x D)	28 m x 0.86 m x 23 cm			28 m x 0.86 m x 23 cm			28 m x 0.86 m x 23 cm			28 m x 0.86 m x 23 cm			28 m x 0.86 m x 23 cm		
Bed Material (D <sub>16</sub> , D <sub>50</sub> , D <sub>84</sub> ) (mm)	-	11.9	-	-	11.7	-	-	11.9	-	-	12.9	-	-	-	-
Pulse Material (D <sub>16</sub> , D <sub>50</sub> , D <sub>84</sub> ) (mm)	-	8.0	-	-	2.8	-	-	8.0	-	-	2.8	-	-	2.8	-
Pulse Mass (kg)	267			267			68			68			68		
Duration (min)	100			100			30			25			25		
Pulse Feed Rate (kg/min)	2.67			2.67			2.27			2.72			2.72		
Average Pre-Pulse Feed Rate (g/min)	0			0			0			0			0		
Pre-Pulse Topography	Plane Bed			Plane Bed			Plane Bed			Plane Bed			Plane Bed		
Mode of Propagation	Both			Both			Both			Both			Both		

**Table 5:** Experimental conditions from Run 5 of this flume study

	<b>Brew et al. (2014)</b>		
Flume Dimensions (L x W x D)	9.14 m x 21.6 cm x 1.50 cm		
Bed Material (D <sub>16</sub> , D <sub>50</sub> , D <sub>84</sub> ) (mm)	0.28 <sup>1</sup>	1.55 <sup>1</sup>	1.90 <sup>1</sup>
Pulse Material (D <sub>16</sub> , D <sub>50</sub> , D <sub>84</sub> ) (mm)	0.86	0.92	0.97
Pulse Mass (kg)	15.69		
Duration (min)	26		
Pulse Feed Rate (kg/min)	0.60		
Average Pre-Pulse Feed Rate (g/min)	0		
Pre-Pulse Topography	Riffle-Pool		
Mode of Propagation	Dispersion		

<sup>1</sup> Surface material gradation reported from surface sampling conducted after Run 2 (Figure 25), after Run 4 visually the bed material appeared even coarser.

### ***Discrepancies between the field and flume experiments***

Our flume experiment was designed to mimic observations on the Elwha and other field situations where artificially high sediment loads have been introduced to an environment with little to no antecedent sediment supply. One of the expected outcomes of the flume experiment was that the sediment pulse would temporarily fill in the pools, as was observed in the months following the removal of Glines Canyon Dam (Figures 15-17). However, both experiments (Runs 3 and 5) resulted in overall aggradation rather than pool filling. This suggests that something other than just increased sediment supply was responsible for the observed changes in the Elwha bed profile. Some of the responsible variables could be a combination of sinuosity, grain size, and hydrology.

Although the flume had width variability, it was not able to meander as a natural river does. A relatively straight reach of the Elwha was selected to be analogous with the flume. However the flow fields and shear stresses created by these meanders are significant and may play at least a minor role in how a system responds to alterations in sediment supply. Field studies have shown that shear stresses are greater on the outside of meander bends due to centrifugal forces causing a superelevated water surface to develop on the bend [Soar and Thorne, 2001]. With greater hydrostatic pressure due to additional depth on the bends outside this zone has the tendency to scour.

In contrast, the zone of maximum sediment transport has been observed to be towards the centerline of the channel as grain effects have been shown to override this hydraulic variability [Dietrich and Smith, 1984]. Secondary circulations have been shown to preferentially push fine particles up the lateral slopes of point bars, while gravitational effects cause coarser particles to roll toward pools [e.g., Dietrich and Smith, 1984].

Analytical theory has shown that the size of point bars in meandering alluvial and mixed bedrock-alluvial channels depends on the average depth, slope, channel curvature, and sediment grain size [Bolla Pittaluga et al. 2009; Nelson et al. 2014]. However, it is a very open question as to how large variable in sediment supply might influence river morphodynamics in curved channels.

The flume experiments in Runs 3 and 5 were designed to transport sediment as bedload only. This is similar to the scenario used in Cui et al. (2003a), where the temporary disappearance of bar topography was observed when finer sediments were transported as bedload. Although it is reasonable to assume that bedload by itself can fill pools under high sediment supply conditions (e.g., Lisle and Hilton, 1992), it is possible that the observed pool filling in the Elwha occurred as a result of deposition of primarily suspended sediment. Recreating that process in the flume setting would likely require sediments that are suspendable at a low discharge. For example, the introduction of low density plastic sediment similar to that used by Braudrick et al. (2009) might have been appropriate to recreate this transient pool filling observed on the Elwha.

Most importantly, variable hydrology was not included in the flume experiment, and this difference is the most likely reason pools filled in on the Elwha but not in the flume. Sediment transport during rising and falling limbs of the hydrograph may produce bed morphology that differs from the equivalent steady flow case as has been shown in experiments by Humphries et al. (2012). It is possible that on the Elwha, the pulse of high sediment supply associated with the dam removal combined with natural hydrographs to produce conditions where sediment was preferentially deposited in pools on the falling limbs of hydrographs during winter storms based on the hydrologic regime depicted in

Figure 18. This sediment could then have been subsequently evacuated from the pools during the rising limb of early summer snowmelt runoff, as the timing of bathymetric surveys on the Elwha suggest.

## CONCLUSIONS

Field observations from the Elwha dam removal project have been used in concert with variable width flume experiments to understand how increased sediment supply interacts with downstream riffle-pool morphology. Flume experiments have shown that introducing a sediment pulse into variable width conditions after prolonged starvation will cause an abrupt adjustment in sediment transport capacity along with a much more efficient dispersion mechanism than a constant width system could provide due to local variabilities in the hydraulics.

A correlation was made between the locations of most constricted channel width and the persistence of pools in variable sediment supply conditions on the Elwha River. Due to the lack of high magnitude peak flows experienced during dam removal, channel variable width appeared to have played an important role in the reemergence of pools as a pulse of sediment was transported through. Unfortunately, the flume experiments in this study were unable to reproduce the temporary pool filling phenomenon observed during the dam removal project, suggesting that width variability is not the sole driver and other fluvial complexities cannot be ignored. Hydrologic variability has been identified as being influential in sediment transport and geomorphic evolution of riverine systems. Therefore unsteady flow appears to be a missing link that must be incorporated to fully understand how a river will accommodate an artificially high sediment load.

Understanding how and why pool filling after dam removal occurs will be important to salmon recovery efforts in coastal river systems. Pools providing critical holding locations for migrating fish to rest in as they navigate upstream to spawning grounds. If

we can understand why temporary pool filling takes place and limit its occurrence during critical migratory time periods, this could improve recovery success rates dramatically.

Results from this study have increased our understanding of how variable width conditions and large alterations in sediment supply interact and have many implications going forward. These findings could benefit from further investigation of sediment pulse evolution in variable width channels with riffle-pool morphology. Building upon this work with experiments that introduce hydrographs and analyze sediment sorting with gravel bed models will be valuable going forward and improve our breadth of knowledge when trying to understand supply and width interactions.

## REFERENCES

- Allan, J. D., & Castillo, M. M. (1995). *Stream ecology* (p. 388). London: Chapman & hall.
- American Rivers. (2014). Frequently Asked Questions. *American Rivers*. Retrieved June 12, 2014, from <http://www.americanrivers.org/initiatives/dams/faqs/>
- Andrews, E. D. (1980). Effective and bankfull discharges of streams in the Yampa River basin, Colorado and Wyoming. *Journal of Hydrology*, 46(3), 311-330.
- Benda, L., & Dunne, T. (1997a). Stochastic forcing of sediment supply to channel networks from landsliding and debris flow. *Water Resources Research*, 33(12), 2849-2863.
- Benda, L., & Dunne, T. (1997b). Stochastic forcing of sediment routing and storage in channel networks. *Water Resources Research*, 33(12), 2865-2880.
- Bittner, L. D., Nino, Y., & Garcia, M. H. (1995). River Bed Response to Channel Width Variation: Theory and Experiments (HES 49).
- Bolla Pittaluga, M., Nobile, G., & Seminara, G. (2009). A nonlinear model for river meandering. *Water Resources Research*, 45(4).
- Bountry, J. (2014). Elwha river restoration sediment effects first two years of dam removal. *RRNW 2014*. Retrieved May 2, 2014, from [http://archive.rrnw.org/docs/2014/11-2\\_Elwha%20Sediment%20Mgmt%20RRNW2014\\_Bountry.pdf](http://archive.rrnw.org/docs/2014/11-2_Elwha%20Sediment%20Mgmt%20RRNW2014_Bountry.pdf)
- Braudrick, C. A., Dietrich, W. E., Leverich, G. T., & Sklar, L. S. (2009). Experimental evidence for the conditions necessary to sustain meandering in coarse-bedded rivers. *Proceedings of the National Academy of Sciences*, 106(40), 16936-16941.
- Bromley, C., Cantelli, A., & Wooster, J. (2011). Summary and synthesis of experimental research on stored sediment response to dam removal. *Sediment Dynamics upon Dam Removal*, 23.
- Buffington, J. M., Lisle, T. E., Woodsmith, R. D., & Hilton, S. (2002). Controls on the size and occurrence of pools in coarse-grained forest rivers. *River Research and Applications*, 18(6), 507-531.
- Bunte, Kristin; Abt, Steven R. (2001). Sampling surface and subsurface particle-size distributions in wadable gravel-and cobble-bed streams for analyses in sediment transport, hydraulics, and streambed monitoring. Gen. Tech. Rep. RMRS-GTR-74. Fort Collins, CO: U.S. Department of Agriculture, Forest Service, Rocky Mountain Research Station. 172.

- Cantelli, A., Paola, C., & Parker, G. (2004). Experiments on upstream-migrating erosional narrowing and widening of an incisional channel caused by dam removal. *Water Resources Research*, 40(3).
- Climate Impacts Group. (2014). *Climate Impacts Group*. Retrieved June 11, 2014, from [http://cses.washington.edu/cig/pnwc/deadend\\_rivertypes.shtml](http://cses.washington.edu/cig/pnwc/deadend_rivertypes.shtml)
- Cui, Y., Parker, G., Lisle, T. E., Gott, J., Hansler-Ball, M. E., Pizzuto, J. E., ... & Reed, J. M. (2003a). Sediment pulses in mountain rivers: 1. Experiments. *Water Resources Research*, 39(9).
- Cui, Y., Parker, G., Pizzuto, J., & Lisle, T. E. (2003b). Sediment pulses in mountain rivers: 2. Comparison between experiments and numerical predictions. *Water Resources Research*, 39(9).
- Cui, Y., & Wilcox, A. (2008). Development and application of numerical models of sediment transport associated with dam removal. *Chapter*, 23, 995-1020.
- Einstein, H. A. (1950). *The bed-load function for sediment transportation in open channel flows* (No. 1026). US Department of Agriculture.
- Ewing, K. (2013, January 1). Riffle, Run, Pool. *Riffles*. Retrieved June 1, 2014, from <http://depts.washington.edu/ehuf473/ehuf473/riffle/run/pool.htm>
- de Almeida, G. A. M., & Rodríguez, J. F. (2011). Understanding pool-riffle dynamics through continuous morphological simulations. *Water Resources Research*, 47(1).
- de Almeida, G. A. M., & Rodríguez, J. F. (2012). Spontaneous formation and degradation of pool-riffle morphology and sediment sorting using a simple fractional transport model. *Geophysical Research Letters*, 39(6).
- Dietrich, W. E., & Smith, J. D. (1984). Bed load transport in a river meander. *Water Resources Research*, 20(10), 1355-1380.
- The Elwha Watershed. (2014, June 14). *National Parks Service*. Retrieved June 17, 2014, from <http://www.nps.gov/olym/naturescience/the-elwha-watershed.htm>
- Fernandez Luque, R., & Van Beek, R. (1976). Erosion and transport of bed-load sediment. *Journal of Hydraulic Research*, 14(2), 127-144.
- Frank, E., & Jørgen, F. (1976). A sediment transport model for straight alluvial channels. *Nordic Hydrology*, 7(5), 293-306.

- The Heinz Center. (2002). *Dam Removal: Science and Decision Making*. Washington D.C.: The H. John Heinz III Center for Science, Economics and the Environment.
- Hey, R. D. (1976). Geometry of river meanders.
- Hey, R. D., & Thorne, C. R. (1986). Stable channels with mobile gravel beds. *Journal of Hydraulic Engineering*, 112(8), 671-689.
- Humphries, R., Venditti, J. G., Sklar, L. S., & Wooster, J. K. (2012). Experimental evidence for the effect of hydrographs on sediment pulse dynamics in gravel-bedded rivers. *Water Resources Research*, 48(1).
- Julien, Pierre Y. (2010). *Erosion and Sedimentation (2nd Edition)*. Cambridge University Press.
- Keller, E. A., & Melhorn, W. N. (1978). Rhythmic spacing and origin of pools and riffles. *Geological Society of America Bulletin*, 89(5), 723-730.
- Keller, E. A., & Swanson, F. J. (1979). Effects of large organic material on channel form and fluvial processes. *Earth surface processes*, 4(4), 361-380.
- Knighton, D. (1998). *Fluvial forms and processes: a new perspective (No. Ed. 2)*. Arnold, Hodder Headline, PLC.
- Lane, E. W. (1955). Design of stable channels, Transactions, ASCE, Paper no. 2776, 20, 1234-1279
- Leopold, L. B., & Wolman, M. G. (1957). *River channel patterns: braided, meandering, and straight (pp. 37-86)*. Washington, DC: US Government Printing Office.
- Leopold, L. B., & Wolman, M. G. Miller] P. 1964. Fluvial processes in geomorphology.
- Leopold, L. B. (1968). Hydrology for urban land planning: A guidebook on the hydrologic effects of urban land use.
- Leopold, L. B. (1994). *A View of the River*. Harvard University Press.
- Lisle, T. E. (1982). Effects of aggradation and degradation on riffle-pool morphology in natural gravel channels, northwestern California. *Water Resources Research*, 18(6), 1643-1651.
- Lisle, T. E. (1986). Stabilization of a gravel channel by large streamside obstructions and bedrock bends, Jacoby Creek, northwestern California. *Geological Society of America Bulletin*, 97(8), 999-1011.

- Lisle, T. E., & Hilton, S. (1992). THE VOLUME OF FINE SEDIMENT IN POOLS: AN INDEX OF SEDIMENT SUPPLY IN GRAVEL-BED STREAMS<sup>1</sup>. *JAWRA Journal of the American Water Resources Association*, 28(2), 371-383.
- Lisle, T. E., Pizzuto, J. E., Ikeda, H., Iseya, F., & Kodama, Y. (1997). Evolution of a sediment wave in an experimental channel. *Water Resources Research*, 33(8), 1971-1981.
- MacWilliams, M. L., Wheaton, J. M., Pasternack, G. B., Street, R. L., & Kitanidis, P. K. (2006). Flow convergence routing hypothesis for pool-riffle maintenance in alluvial rivers. *Water Resources Research*, 42(10).
- Montgomery, D. R., Buffington, J. M., Smith, R. D., Schmidt, K. M., & Pess, G. (1995). Pool spacing in forest channels. *Water Resources Research*, 31(4), 1097-1105.
- Montgomery, D. R., & Buffington, J. M. (1997). Channel-reach morphology in mountain drainage basins. *Geological Society of America Bulletin*, 109(5), 596-611.
- Nelson, P. A., Venditti, J. G., Dietrich, W. E., Kirchner, J. W., Ikeda, H., Iseya, F., & Sklar, L. S. (2009). Response of bed surface patchiness to reductions in sediment supply. *Journal of Geophysical Research: Earth Surface (2003–2012)*, 114(F2).
- Nelson, P. A., & Seminara, G. (2011). Modeling the evolution of bedrock channel shape with erosion from saltating bed load. *Geophysical Research Letters*, 38(17).
- Richards, K. S. (1976). The morphology of riffle-pool sequences. *Earth Surface Processes*, 1(1), 71-88.
- Richards, K. (1982). *Rivers from and process in alluvial channels*. Methuen.
- Schumm, S. A. (1977). *The fluvial system* (Vol. 338). New York: Wiley.
- Schwartz, J. (2013, September 11). Park Service, Port Angeles agree to water treatment fix. *Peninsula Daily News*. Retrieved April 2, 2014, from <http://www.peninsuladailynews.com/article/20130912/news/309129985/park-service-port-angeles-agree-to-water-treatment-fix>
- Shields, A. (1936). Application of similarity principles and turbulence research to bed-load movement.
- Sklar, L. S., Fadde, J., Venditti, J. G., Nelson, P., Wydzga, M. A., Cui, Y., & Dietrich, W. E. (2009). Translation and dispersion of sediment pulses in flume experiments simulating gravel augmentation below dams. *Water resources research*, 45(8).

- Smillie, J. (2014, March 30). Federal judge sides with wild-fish advocates on hatchery issue in Elwha River's restoration. *Peninsula Daily News*. Retrieved June 4, 2014, from <http://www.peninsuladailynews.com/article/20140330/news/303309972/federal-judge-sides-with-wild-fish-advocates-on-hatchery-issue-in>.
- Soar, P. J., & Thorne, C. R. (2001). *Channel restoration design for meandering rivers* (No. ERDC/CHL-CR-01-1). ENGINEER RESEARCH AND DEVELOPMENT CENTER VICKSBURG MS COASTAL AND HYDRAULICSLAB.
- Swanson, F. J., Lienkaemper, G. W., & Sedell, J. R. (1976). History, physical effects, and management implications of large organic debris in western Oregon streams.
- Thompson, D. M., Wohl, E. E., & Jarrett, R. D. (1996). A revised velocity-reversal and sediment-sorting model for a high-gradient, pool-riffle stream. *Physical Geography*, 17(2), 142-156.
- Thompson, D. M., Wohl, E. E., & Jarrett, R. D. (1999). Velocity reversals and sediment sorting in pools and riffles controlled by channel constrictions. *Geomorphology*, 27(3), 229-241.
- Thompson, D. M., & Wohl, E. E. (2009). The linkage between velocity patterns and sediment entrainment in a forced-pool and riffle unit. *Earth Surface Processes and Landforms*, 34(2), 177-192.
- Thorne, C. R., Hey, R. D., & Newson, M. D. (1997). *Applied fluvial geomorphology for river engineering and management*. John Wiley & Sons Ltd.
- Venditti, J. G., Nelson, P. A., Minear, J. T., Wooster, J., & Dietrich, W. E. (2012). Alternate bar response to sediment supply termination. *Journal of Geophysical Research: Earth Surface* (2003–2012), 117(F2).
- White, J. Q., Pasternack, G. B., & Moir, H. J. (2010). Valley width variation influences riffle-pool location and persistence on a rapidly incising gravel-bed river. *Geomorphology*, 121(3), 26-221.
- Williams, G. P. (1978). Bank-full discharge of rivers. *Water resources research*, 14(6), 1141-1154.
- Wong, M., & Parker, G. (2006). Reanalysis and correction of bed-load relation of Meyer-Peter and Müller using their own database. *Journal of Hydraulic Engineering*, 132(11), 1159-1168.

Wu, F. C., & Yeh, T. H. (2005). Forced bars induced by variations of channel width: Implications for incipient bifurcation. *Journal of Geophysical Research: Earth Surface* (2003–2012), 110(F2).

APPENDIX A

Nays Numerical Validation – Bittner et al. (1995)

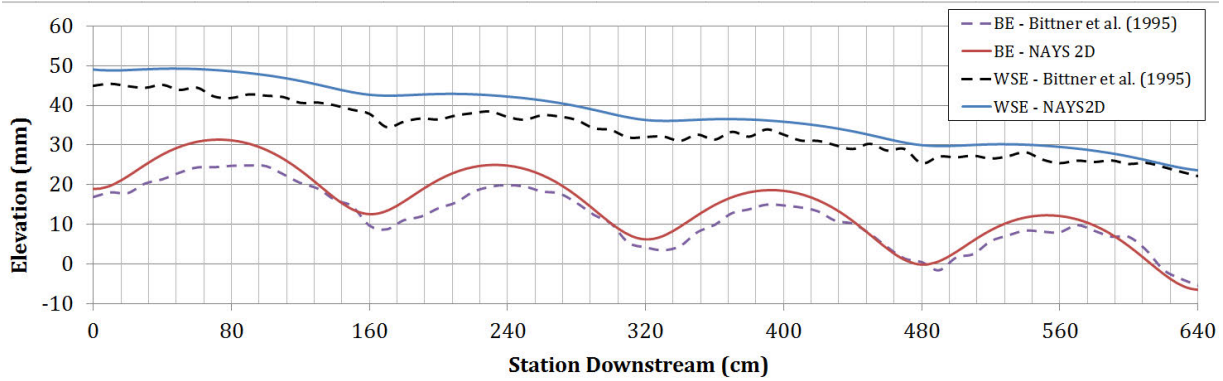


Figure 41: Comparison of measured bed and water surface profiles by Bittner et al. (1995) to those modeled in Nays2D.

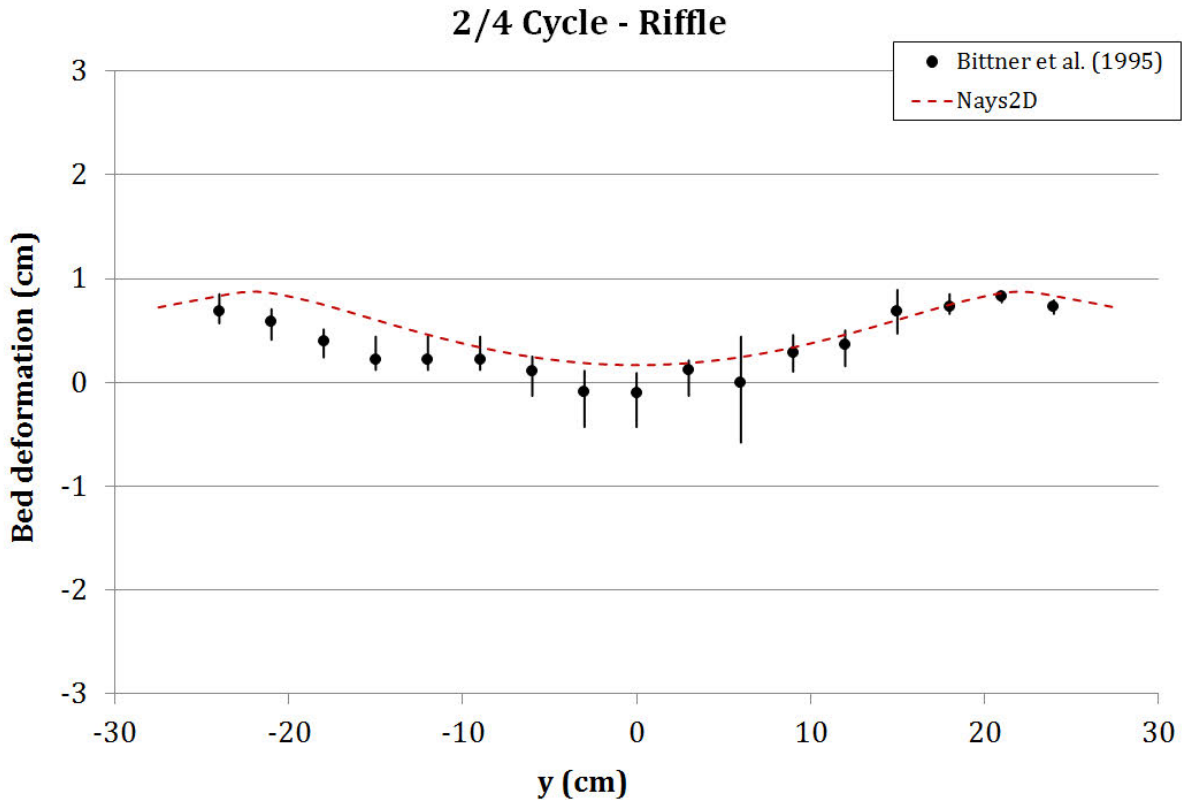
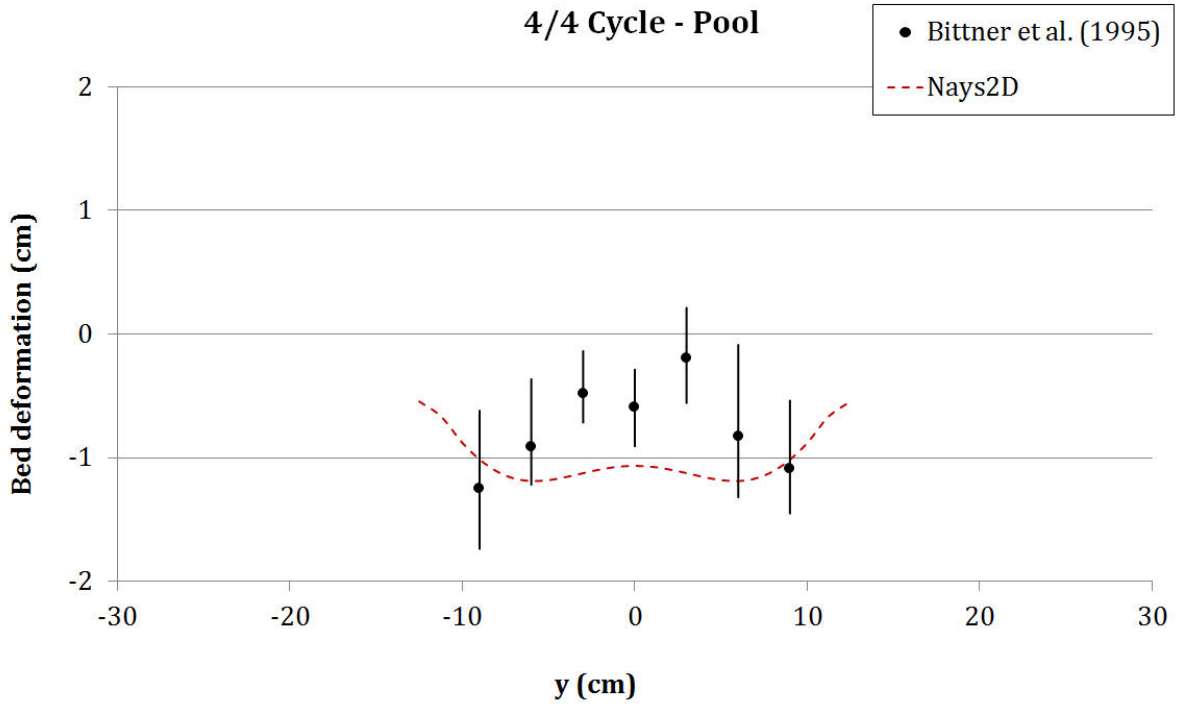


Figure 42: Comparison of measured riffle cross sectional deformation by Bittner et al. (1995) to that modeled in Nays2D.



**Figure 43:** Comparison of measured pool cross sectional deformation by Bittner et al. (1995) to that modeled in Nays2D.

APPENDIX B

Water Surface and Bed Profiles - Run 1

Distance Upstream (mm)	Survey Start Time						Notes
	2:38 PM		3:57 PM		5:00 PM		
	Time Elapsed						
	10.13		11.45		12.50		
	Bed (mm)	WS (mm)	Bed (mm)	WS (mm)	Bed (mm)	WS (mm)	
7657	105.156	120.396	87.478	116.738	101.194	117.653	Wall Entrance
7387	102.108	116.738	83.820	114.605	96.317	113.995	
7117	99.060	111.252	84.125	110.947	90.221	110.642	Narrow
6847	100.584	109.728	88.392	108.814	89.916	108.814	
6577	102.108	111.862	89.002	108.814	90.221	107.290	Wide
6307	96.012	107.533	83.820	106.375	86.258	105.766	
6037	92.964	107.290	80.162	102.108	82.906	101.498	Narrow
5747	92.354	104.546	79.248	101.498	81.077	101.498	
5477	89.306	99.060	80.772	98.450	81.077	96.926	Wide
5207	92.050	100.279	61.874	97.536	79.248	99.670	
4937	74.066	93.878	61.265	85.039	74.371	92.050	Narrow
4667	78.334	96.317	61.874	92.964	74.066	95.402	
4397	77.419	93.574	72.847	92.050	74.981	89.916	Wide
4127	75.590	93.574	71.018	91.745	70.409	92.964	
3857	72.238	90.221	70.714	87.478	66.142	87.782	Narrow
3587	75.286	89.002	60.046	87.782	65.837	84.734	
3317	73.762	86.258	60.960	86.258	67.970	86.868	Wide
3047	74.066	84.734	60.350	84.125	67.970	86.258	
2777	64.922	80.467	50.292	81.382	59.741	80.162	Narrow
2507	63.094	81.077	55.169	78.943	60.046	81.382	
2237	72.542	78.943	60.046	80.162	61.874	79.553	Wide
1967	61.874	76.200	47.244	77.419	61.570	78.334	
1697	59.131	73.762	37.490	74.066	54.864	74.981	Narrow
1427	63.094	73.762	35.052	72.542	53.950	74.371	
1157	56.388	73.457	33.833	71.628	56.693	73.457	Wall Exit
717	56.693	73.152	47.854	72.238	53.645	71.018	Exit Reach

### Water Surface Profiles - Run 2

Distance Upstream (mm)	Date/Time							Notes
	4/21/2014	4/21/2014	4/22/2014	4/22/2014	4/23/2014	4/24/2014	4/28/2014	
	11:02 AM	4:12 PM	10:24 AM	2:12 PM	12:05 PM	10:58 AM	4:55 PM	
	Time Elapsed (hrs)							
	0.87	2.18	4.37	6.43	10.68	14.90	23.58	
	WS (mm)							
8277	-	-	-	-	-	-	101.194	Entrance Reach
7657	110.033	103.632	100.279	96.926	96.012	94.793	94.793	Wall Entrance
7387	106.680	98.450	96.012	92.659	89.611	89.306	88.697	
7117	104.851	101.194	96.317	91.440	90.526	89.916	89.002	Narrow
6847	102.718	96.926	93.878	92.964	89.002	88.392	87.782	
6577	100.889	98.450	92.354	91.745	88.697	87.173	87.478	Wide
6307	102.718	96.012	92.659	90.221	85.649	85.039	85.344	
6037	96.926	90.830	92.354	89.916	86.563	84.734	85.344	Narrow
5747	96.012	89.916	86.868	.	84.734	84.734	83.820	
5477	94.488	91.135	88.392	86.868	82.601	86.563	81.686	Wide
5207	92.050	87.782	89.002	83.515	83.210	84.125	78.638	
4937	89.611	84.734	81.077	82.906	77.114	77.724	77.114	Narrow
4667	89.306	84.125	84.430	78.943	78.334	77.114	80.467	
4397	88.392	85.954	83.210	81.077	79.858	78.334	80.467	Wide
4127	87.173	84.125	81.382	80.467	78.638	77.114	77.419	
3857	85.649	79.858	80.467	76.200	78.334	77.419	77.724	Narrow
3587	83.820	80.772	78.029	77.114	74.066	77.724	75.286	
3317	85.344	78.638	78.029	74.676	74.981	76.505	74.371	Wide
3047	81.382	79.248	78.029	75.590	74.676	74.981	74.066	
2777	81.382	75.590	74.981	71.018	71.628	73.762	73.762	Narrow
2507	74.981	74.676	69.494	73.457	70.104	72.542	70.104	
2237	78.334	74.676	69.190	69.190	71.018	71.018	69.494	Wide
1967	74.066	75.895	70.104	66.142	71.323	70.104	69.190	
1697	73.457	72.542	71.018	69.190	68.885	69.494	69.190	Narrow
1427	72.542	71.628	66.751	67.970	65.837	69.799	67.666	
1157	71.018	72.238	67.970	65.227	66.142	69.190	66.446	Wall Exit
717	67.970	67.970	67.666	64.008	65.837	66.751	68.275	
367	67.970	65.532	64.618	63.398	64.313	-	-	
317	-	-	-	-	-	66.142	65.227	Exit Reach

APPENDIX C



**Figure 44:** Surface material at riffle location after Run 1 (13 hours).



**Figure 45:** Surface material at riffle location after Run 2 (24.13 hours).

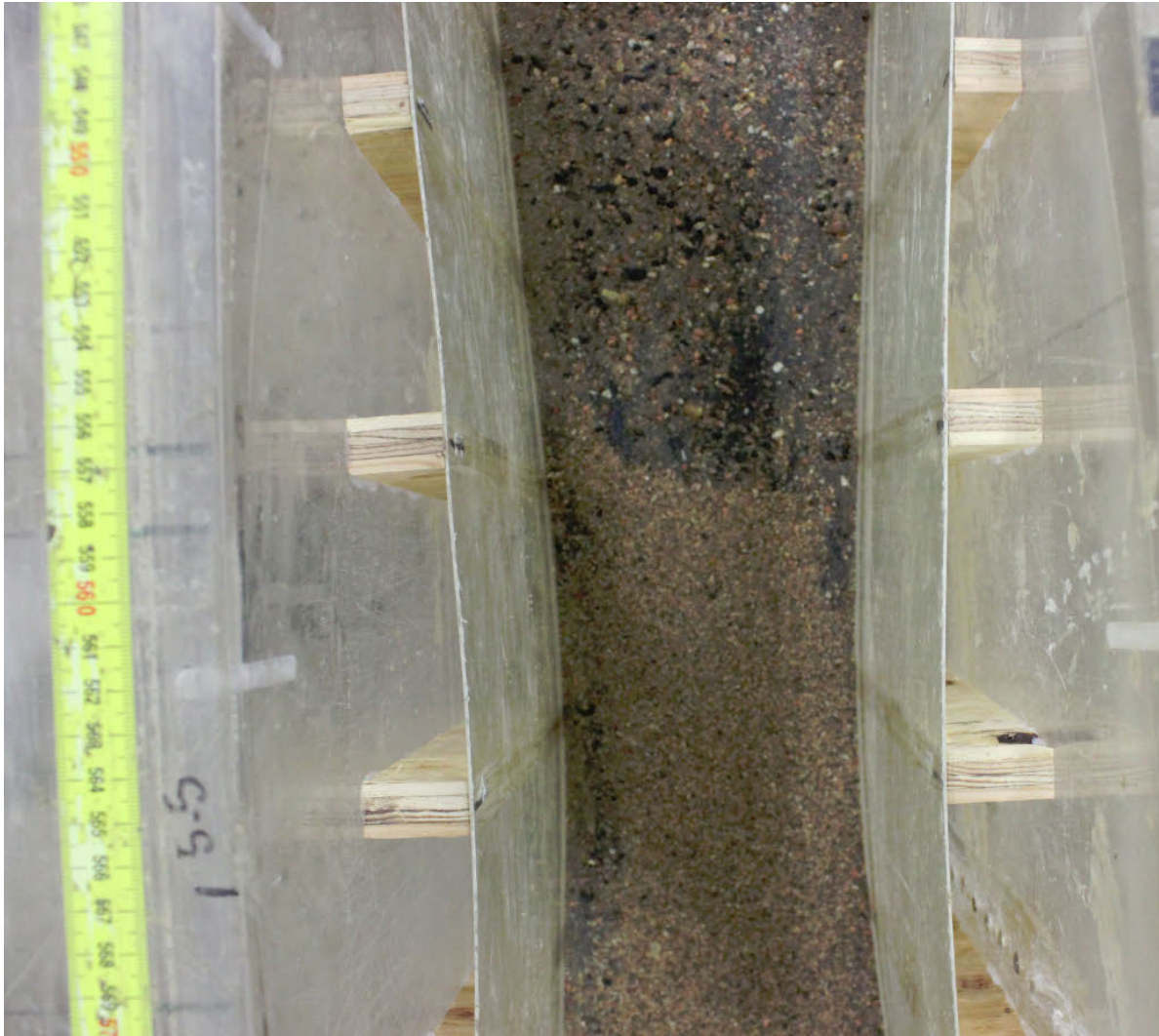


**Figure 46:** Location of fine sediment pulse front after 10 minutes (Run 5).



**Figure 47:** Location of sediment pulse after 27 minute (Run 5).

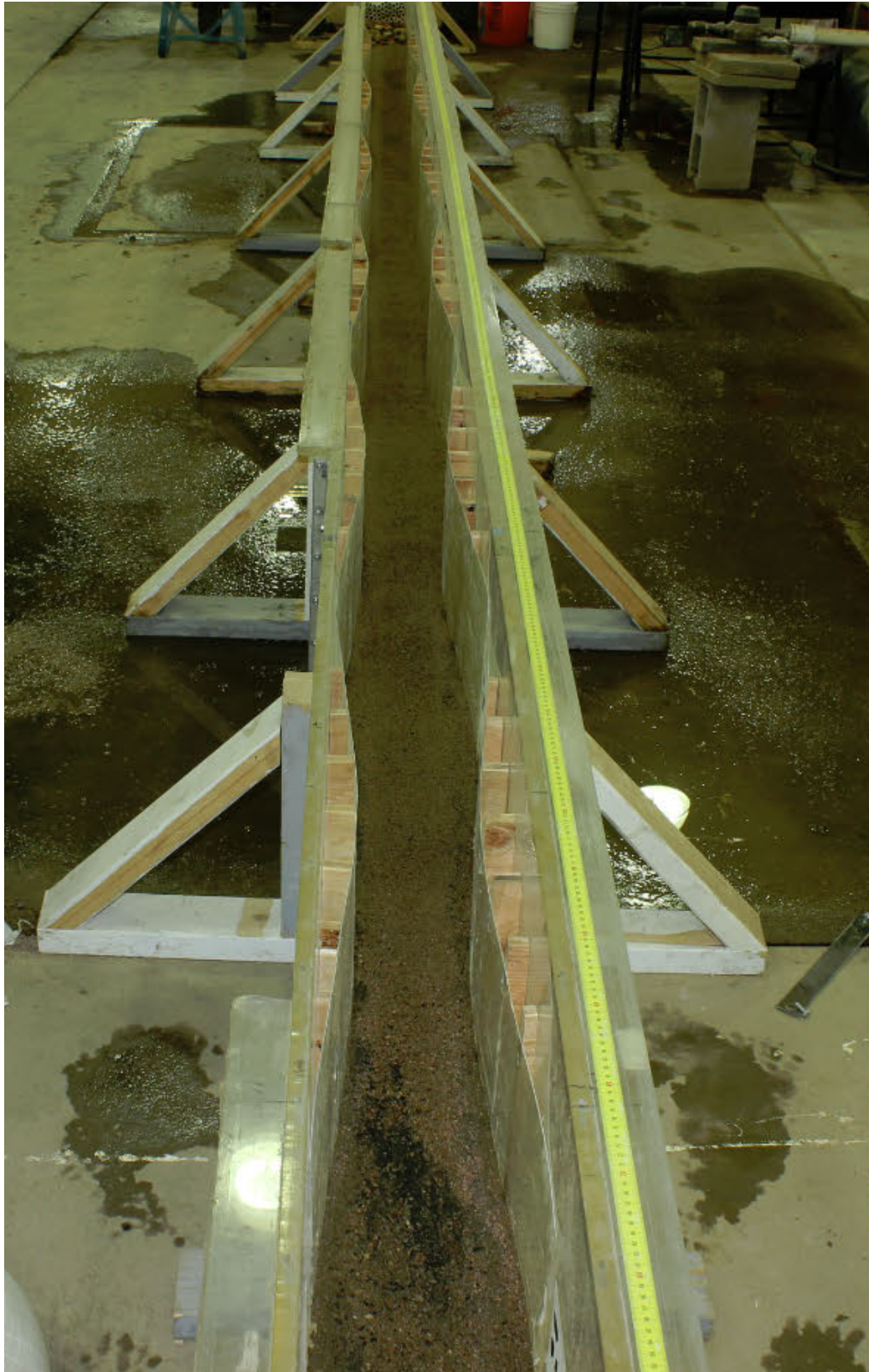


**Figure 48:** Sediment pulse front after 47 minutes (Run 5).



**Figure 49:** Sediment Pulse after reaching the flume outlet at 86 minutes.



**Figure 50:** Return to an armored condition after 711 minutes (Run 5).